GPM Combined Radar-Radiometer Precipitation Algorithm Theoretical Basis Document (Version 2)

Willam S. Olson, Hirohiko Masunaga

and the

GPM Combined Radar-Radiometer Algorithm Team

November 30, 2011

Table of Contents

1. Introduction

The GPM Combined Radar-Radiometer Algorithm performs two basic functions: first, it provides, in principle, the most accurate, high resolution estimates of surface rainfall rate and precipitation vertical distributions that can be achieved from a spaceborne platform, and it is therefore valuable for applications where information regarding instantaneous storm structure are vital. Second, a global, representative collection of combined algorithm estimates will yield a single common reference dataset that can be used to "cross-calibrate" rain rate estimates from all of the passive microwave radiometers in the GPM constellation. The cross-calibration of radiometer estimates is crucial for developing a consistent, high time-resolution precipitation record for climate science and prediction model validation applications. Because of the Combined Algorithm's essential roles as accurate reference and calibrator, the GPM Project is supporting a Combined Algorithm Team to implement and test the algorithm prior to launch. In the pre-launch phase, GPM-funded science investigations may lead to significant improvements in algorithm function, but the basic algorithm architecture has been formulated. This algorithm architecture is largely consistent with the successful TRMM Combined Algorithm design, but it has been updated and modularized to take advantage of improvements in the representation of physics, new climatological background information, and model-based analyses that may become available at any stage of the mission. This document presents a description of the GPM Combined Algorithm architecture, scientific basis, supporting ancillary datasets, inputs/outputs, and testing plan.

2. Background

GPM Instruments

The GPM core mission satellite observatory is shown in Fig. 1. From this platform, the Dual-frequency Precipitation Radar (DPR) scans cross-track in relatively narrow swaths at Ku band (13.6 GHz) and Ka band (35.5 GHz). The dual-frequency radar reflectivity observations are nearly beam-matched over the 125 km Ka-band swath, with a horizontal resolution of approximately 5 km, and a vertical resolution of 250 m in standard observing mode. The Ku band radar scans over a wider, 245 km swath. The GPM Microwave Imager (GMI) scans conically over an 885 km wide swath at frequencies of 10.65, 18.7, 23.8, 36.5, 89.0, 165.5, 183.31 ± 7, and 183.31 ± 3 GHz. Measured brightness temperatures are in two polarizations (vertical and horizontal) at all but the 23.8 GHz and 183.3 GHz channels, which provide only vertical polarization measurements. The GMI observations are diffraction limited, with the lowest-resolution footprints (approx. 26 km) at 10.7 GHz and the highest-resolution footprints (approx. 6 km) at the 89.0 GHz and higher frequency channels.

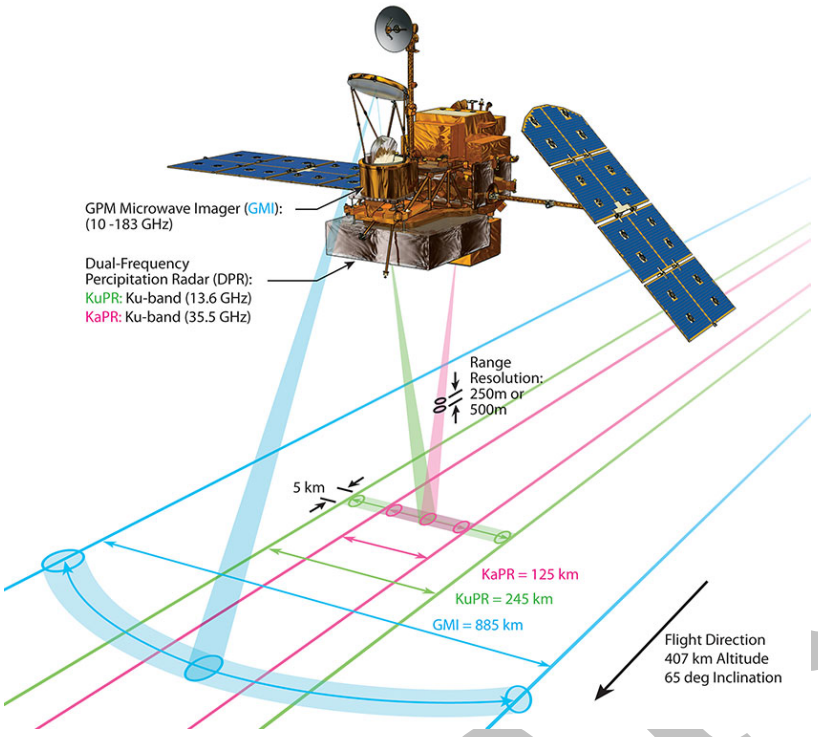

Fig. 1. Configuration of the GPM core observatory, illustrating the scanning geometry of the DPR and GMI instruments.

Implications for Algorithm Design

The current GPM Combined Radar-Radiometer Algorithm architecture is descended from a rich heritage of algorithms that were developed for the TRMM mission, as well as other algorithms developed and applied to airborne radar-radiometer data. In TRMM, only Ku-band radar observations were available from the radar instrument (the Precipitation Radar, or PR), and only lower-frequency ($\leq$ 85 GHz) brightness temperature measurements were available from the microwave radiometer (the TRMM Microwave Imager, or TMI). The TRMM Facility Combined Algorithm used radiometer information to essentially reduce uncertainties in estimates of radar-derived total path-integrated attenuation to the earth's surface to perform an improved attenuation correction of the radar reflectivity vertical profile. The improved attenuation correction was effected by adjusting a single parameter of the precipitation particle-size distribution over the entire precipitation vertical profile. This single parameter represented a rain-normalized, mass-weighted mean particle diameter, which was assumed to be locally constant over the scale of TMI footprints. Adding horizontal variations of this parameter would have introduced too many free parameters to the inversion problem.

The GPM Combined Algorithm takes advantage of the additional information provided by the Ka band radar channel to glean more specific information about the precipitation size distribution and associated attenuation in each gate. The estimation of precipitation size distribution parameters is further aided by precipitation attenuation information from the GMI channels, which have an extended spectral

range relative to the TMI. However, if the Ka band reflectivities do not provide additional information due to very light rain (Rayleigh limit), or they are severely attenuated in heavy precipitation, then the combined algorithm must make a natural transition to a single-frequency, Ku band solution in which a more approximate estimation of precipitation size distribution parameters is performed.

Regardless of whether or not the Ka band data are applicable, however, information from the GMI brightness temperatures can be used to make further adjustments of path attenuation due to non-precipitating cloud liquid water and water vapor, which are not directly sensed by the DPR. In addition, there are precipitation microphysical parameters, such as the intercept of the particle size distribution and the density of ice-phase precipitation that may be adjusted using radiometer information.

Ultimately, the degree to which any precipitation or environmental parameters can be adjusted is limited by the information content of the DPR and GMI observations and any additional information provided by *a priori* data, such as the natural ranges of particle size distribution parameters, cloud water contents, etc., and how these parameters covary spatially. Therefore, as outlined in section 3, the combined algorithm is designed to be able to accept both different physical modeling assumptions and *a priori* constraints on estimated parameters.

3. Algorithm Architecture

Overview

The current algorithm design is based upon an Ensemble Kalman Filtering (EnKF) approach for inverting the DPR reflectivities and GMI brightness temperatures to estimate precipitation profiles; see Anderson (2003) for a general description of EnKF approaches. The general architecture of the GPM Combined Algorithm is illustrated in Fig. 2a-d. There are three primary modules in the Combined Algorithm: an Environment Module, which establishes the environmental background of the precipitation distributions to be estimated, a Radar Module, which produces ensembles of radar-consistent precipitation profile solutions at each DPR footprint location, and a Radiometer Module, that modifies the radar-derived precipitation ensembles to be more consistent with the GMI observations. The outputs of the algorithm are the mean (best estimate) and standard deviation (uncertainty of estimate) of the DPR-GMI filtered ensemble of estimated precipitation profiles at each DPR footprint location. Following is a description of the algorithm flow from the ingest of satellite sensor data to the output of precipitation estimates.

The Environment Module (Fig. 2a) first ingests DPR Level 2 calibrated reflectivities at Ku and Ka band (if available) as well as Level 1C intercalibrated brightness temperatures from the GMI. To stay within computer memory limitations, a maximum of 300 scan lines of DPR data and corresponding GMI data are processed by the algorithm at a time. Therefore, the flow diagram of Fig. 2 represents the processing of one swath segment, which is repeated until the entire orbit is processed.

The DPR footprint locations define an approximate 5 km x 5 km grid on the earth's surface, and these footprints are used to represent the solution grid for algorithm-estimated precipitation profiles.

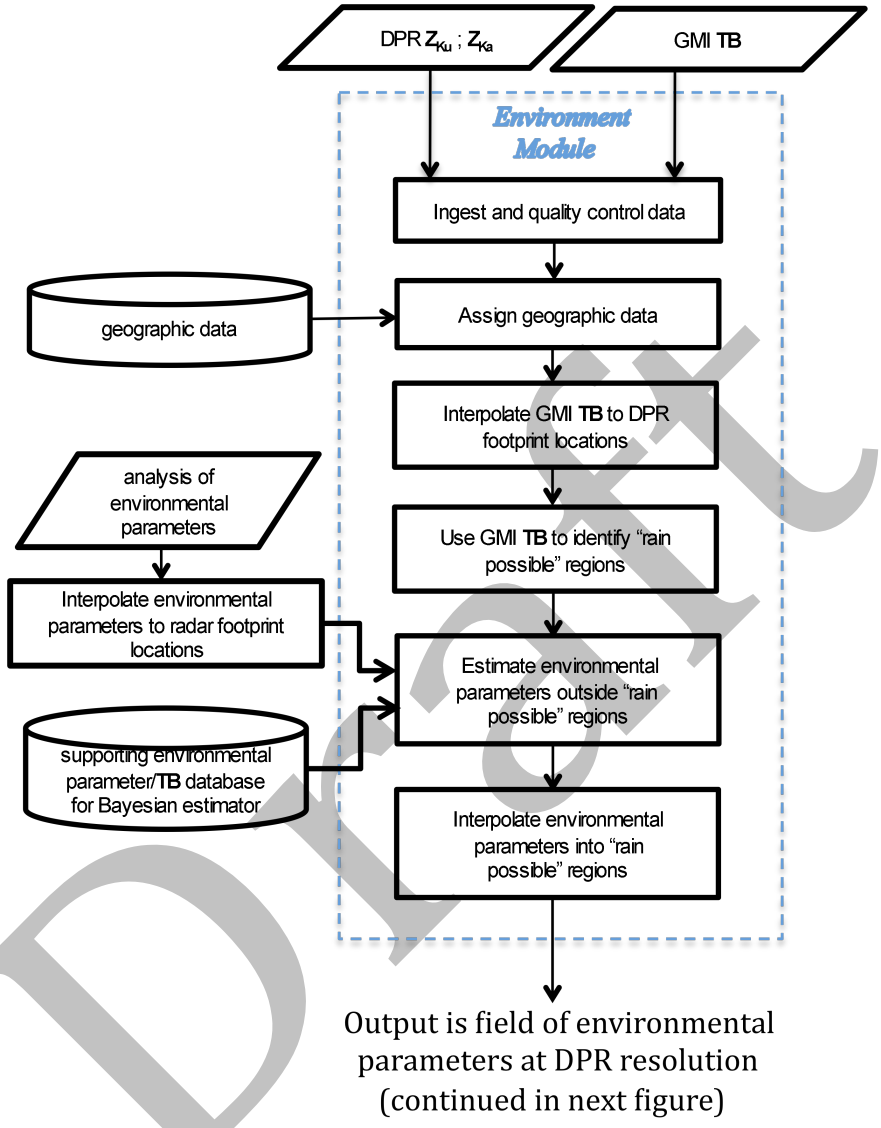

Fig. 2a. Environment Module processing schematic of the Combined Radar-Radiometer Algorithm.

The next step is to assign surface water fraction and elevation values to the DPR footprint locations. Surface water fraction and elevation values are drawn from a static geographic database and interpolated to the DPR footprint locations. Currently, both DPR and GMI data are utilized to estimate precipitation profiles over open ocean locations, while only DPR data are utilized over other surfaces. The use of GMI data over non-ocean surfaces will be implemented in the next algorithm version.

To create a uniform grid of input data, the GMI brightness temperatures (**TB**) are interpolated from the GMI scans to the DPR footprint locations. A screening method is then applied to the GMI data to determine if precipitation is "possible" at each footprint location. The screening method is derived from the GPROF Algorithm V6 methodology; see McCollum and Ferraro (2005). If precipitation is not possible according to the screening method, a Bayesian estimator is applied to the interpolated **TB** data to derive environmental parameters. The Bayesian estimator has the form

$$\begin{pmatrix} TPW \\ CLWP \\ Tsfc \\ U10m \end{pmatrix} = \frac{1}{\Lambda} \sum_{j}^{ocean\ dbase} \begin{pmatrix} TPW_j \\ CLWP_j \\ Tsfc_j \\ U10m_j \end{pmatrix} \times \exp\left\{-0.5\left(\mathbf{TB}_j - \mathbf{TB}_{obs}\right)^T \mathbf{W}_{\mathbf{TB}}^{-1}\left(\mathbf{TB}_j - \mathbf{TB}_{obs}\right)\right\} \quad (1)$$

$$\times \exp\left\{-0.5\left(TPW_j - TPW_{anal}\right)^T W_{TPW}^{-1}\left(TPW_j - TPW_{anal}\right)\right\}$$
$$\times \exp\left\{-0.5\left(CLWP_j - CLWP_{anal}\right)^T W_{CLWP}^{-1}\left(CLWP_j - CLWP_{anal}\right)\right\}$$
$$\times \exp\left\{-0.5\left(Tsfc_j - Tsfc_{anal}\right)^T W_{Tsfc}^{-1}\left(Tsfc_j - Tsfc_{anal}\right)\right\}$$
$$\times \exp\left\{-0.5\left(U10m_j - U10m_{anal}\right)^T W_{U10m}^{-1}\left(U10m_j - U10m_{anal}\right)\right\}$$

where *TPW* is the total precipitable water in the atmospheric column, *CLWP* is the cloud liquid water path in the column, *Tsfc* is the surface skin temperature, and *U10m* is the wind speed at 10-m altitude. The GMI observed brightness temperatures are symbolized by $\mathbf{TB}_{\mathbf{obs}}$. The Bayesian estimator is supported by a database of atmospheric profiles and corresponding simulated brightness temperatures indexed by *j*; therefore TPW_j, $CLWP_j$, $Tsfc_j$, and $U10m_j$ are the environmental parameters associated with database profile *j*, and $\mathbf{TB}_j$ are the corresponding simulated upwelling brightness temperatures for that profile. The uncertainties of observed and database values of the parameters are included in the error covariance matrices, W, and Λ is a normalization factor. In addition to the GMI observed $\mathbf{TB}_{\text{obs}}$, the Bayesian estimates can be constrained by *a priori* estimates of TPW_{anal}, $CLWP_{anal}$, $Tsfc_{anal}$, and $U10m_{anal}$, which are derived from the DPR Level 2 algorithm. The impact of this analysis information is under study. The databases and analysis information supporting the estimation of environmental parameters are described in section 4.

After the environmental parameters are estimated in regions where rain is not possible, they are linearly interpolated into the regions where is rain is possible, creating a complete field of environmental parameters on the DPR grid.

The Radar Module (Fig. 2b) ingests all output from the Environment Module, including the fields of GMI-derived environmental parameters on the DPR grid. In regions where precipitation is detected, the interpolated estimates of water vapor, cloud water, surface skin temperature, and 10-m wind speed are derived from relatively coarse-scale GMI observations (~15 km) in non-precipitating conditions, and therefore it is not expected that the interpolated estimates will accurately

represent conditions in precipitating clouds at the spatial resolution of the DPR grid (5 km). For example, water vapor and cloud amounts may be enhanced in precipitation regions relative to their surroundings. Moreover, even if the environment of a given radar profile is correctly specified, it is not evident that all parameters describing the precipitation size distribution (PSD) in each radar range bin can be retrieved from the Ku- and Ka-band reflectivity profiles at that location.

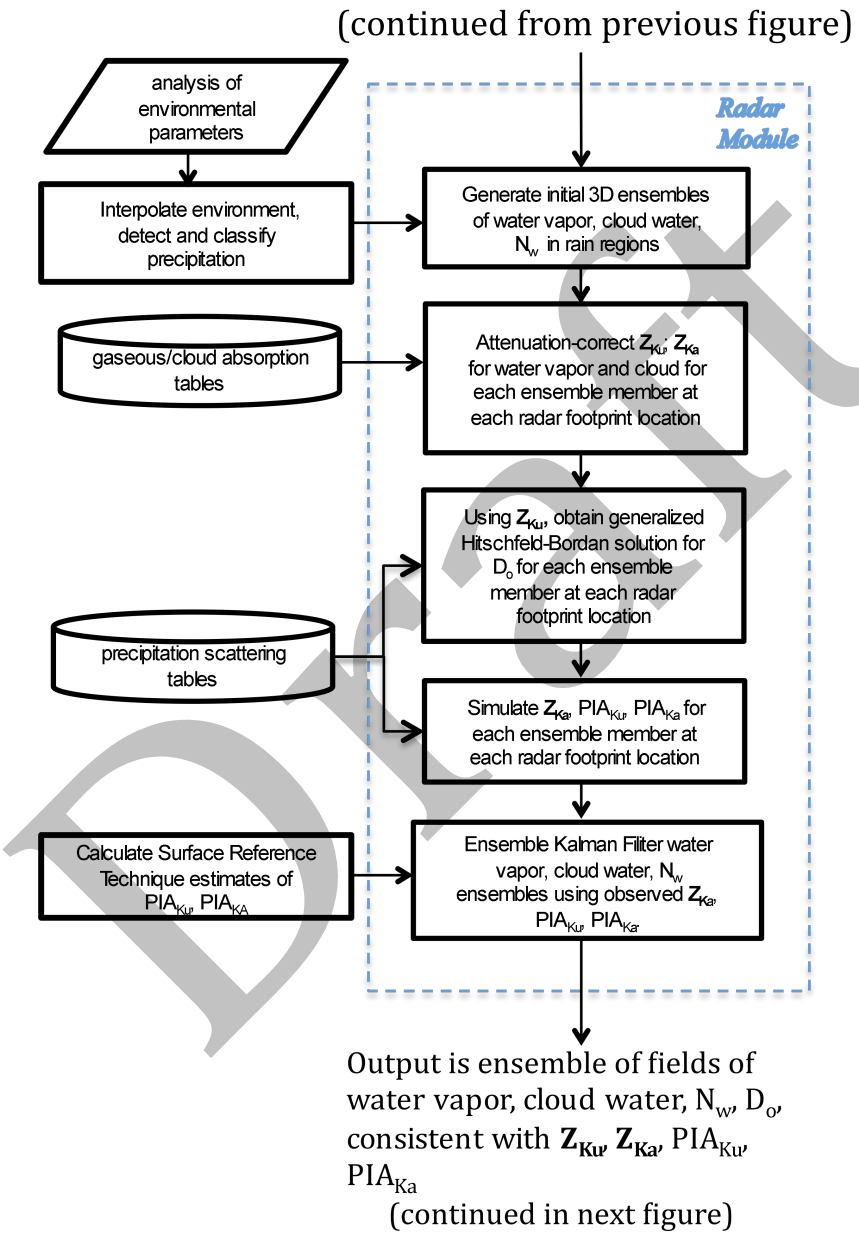

Fig. 2b. Radar Module processing schematic of the Combined Radar-Radiometer Algorithm.

Therefore, to represent the *a priori* distributions of environmental and PSD parameters at each DPR footprint location where precipitation is detected, ensembles

of 3D parameter fields are generated. Typically, 50-member ensembles of these parameter fields are generated; only a coarse representation of any *a priori* pdf's of the parameters are needed, since subsequent EnKF filtering of the ensembles will effectively modify the original pdf's to create new, "interpolated" pdf's of the parameter fields consistent with the observations. A detailed description of the filtering will follow in this subsection.

The 3D ensembles of environmental parameters in precipitation regions can be generated based upon the interpolated GMI estimates or derived independently. Different methods for generating the 3D ensembles are under investigation. Currently, the *Tsfc* and *U10m* values spatially interpolated from the GMI estimates are specified for all ensemble members, and pressure and temperature vertical profiles are parameterized as functions of *Tsfc*. On the other hand, water vapor and cloud water vertical profiles are currently drawn from static CRM-generated databases that represent the region of algorithm application, and these profiles are assigned to DPR footprint locations to create the 3D ensembles. The water vapor density profile, $\mathbf{q_v}$, and cloud water content profile, $\mathbf{q_{cld}}$, are randomly assigned to each ensemble member from distributions of profiles stored in the static database. The atmospheric profiles are re-sampled in the vertical at the nominal bin resolution of the DPR (250 m).

To the 3D ensembles of *Tsfc*, *U10m*, pressure, temperature, water vapor, and cloud water are added PSD parameters at the nominal radar bin resolution. It is assumed that the precipitation particle size distribution in each bin is described by a normalized gamma distribution (Testud et al. 2000),

$$n(D) = N_w \, f(\mu) \left(\frac{D}{D_o} \right)^{\mu} \exp\left(-\frac{(3.67+\mu)}{D_o} D \right), \tag{2}$$

where

$$f(\mu) \;=\; \frac{6(3.67+\mu)^{\mu+4}}{3.67^4 \, \Gamma(\mu+4)} \,. \tag{3}$$

Here, N_w is the intercept of the normalized distribution, D_o is the median volume diameter, μ is the distribution shape factor, D is the liquid-water equivalent diameter of the particle, and $n(D)$ is the spectral number density of particles with diameter D. Since there are at most two independent radar-derived reflectivity observations associated with each DPR range bin, the solution strategy is to fix one of the three free parameters of the size distribution, allow a second that varies slowly in space to be modified by the EnKF filtering, and determine a third using the radar data, since the first two parameters are defined for a given ensemble member. In the current algorithm, μ is assumed constant across all of the ensembles. An autoregressive function is used to generate N_w values in each profile, starting with a random value drawn from an assumed pdf at the top of the profile. These profiles of N_w are randomly assigned at a sample spacing coarser than the DPR grid and then

interpolated to the DPR footprint locations. The purpose of the autoregressive generation and spatial interpolation of N_w profiles is to create correlated values of N_w across the precipitation field in any given ensemble member, since such correlations are observed in field studies; e.g., Tokay and Bashor (2010); Thurai et al. (2011). Fixing μ and imposing spatial correlations on N_w values helps to limit the effective number of free parameters in the estimation problem. The third parameter, D_o, in each range bin is inverted from the profile of Ku band reflectivities and the given ensemble member profiles of μ and N_w at each DPR footprint location, as described forthwith.

To estimate the PSD parameters at each DPR footprint location, the reflectivity profiles at Ku and Ka band are first corrected for gaseous and cloud water attenuation in each of the 50 ensemble member environmental profiles. The specific absorption by atmospheric gases and cloud water as a function of pressure, temperature, humidity and cloud water content is drawn from tabulated values at the Ku and Ka band frequencies. The remaining attenuation in each ensemble member reflectivity profile is due to precipitation.

Using the gas/cloud absorption-corrected Ku reflectivity profile ($\mathbf{Z_{Ku}}$) associated with a given ensemble member, a generalized Hitschfeld-Bordan method is applied to solve for the profile of D_o for that member; see Grecu et al. (2011). The generalized Hitschfeld-Bordan method is a single-wavelength, forward recursive method that iteratively computes the effective reflectivity and extinction by precipitation in a given range bin; then attenuation-corrects the reflectivity in the next range bin of the profile; see Fig. 2d. In the generalized approach, the iteration of reflectivity and extinction calculations is made computationally efficient through an analytical manipulation of the radar equation; see Grecu et al. (2011). The iteration equation is

$$Z(r) = \frac{Z_{Ku}(r)}{\left[1 - q\int_0^r Z_{Ku}^{\beta}(s)\frac{k\left(Z(s)\right)}{Z^{\beta}(s)}ds\right]^{1/\beta}}, \qquad (4)$$

where $Z(r)$ is the attenuation-corrected reflectivity at range r, $Z_{Ku}(r)$ is the measured reflectivity at that range, $k(Z)$ is the specific extinction corresponding to reflectivity Z, $q = 0.2\ \beta \ln(10)$, and $k = \alpha\ Z^{\beta}$ is an approximate k-Z relation that it introduced to reduce the number of iteration steps. The actual relationships between precipitation extinction and reflectivity are represented by static "scattering" tables of these quantities for a range of N_w and D_o values, given μ. In high-attenuation regimes, numerical instabilities are avoided by rescaling the N_w profile; see Fig. 2d. The generalized Hitschfeld-Bordan method is applied to all of the member profiles in the ensemble at each Ku-band footprint location.

Next, if valid Ka-band data exist at a given Ku-band footprint location, the ensemble of Ku-band precipitation profile solutions is used to simulate a corresponding ensemble of Ka-band reflectivity profiles and total path-integrated attenuations (*PIA*'s) at Ku and Ka band. Again, the scattering tables are used to relate

the Ku-band estimated precipitation profiles to the simulated reflectivities and *PIA*'s. The covariances between the unknown $\mathbf{q_v}$, $\mathbf{q_{cld}}$, $\mathbf{ln(N_w)}$ and the simulated observations are then computed from the ensembles of these parameters. The ensemble covariances describe how variations of the unknown parameters in the ensemble should relate to variations in observed reflectivities at Ka band, $\mathbf{Z_{Ka}}$, as well as observed *PIA*'s at Ku and Ka band, PIA_{Ku} and PIA_{Ka}, respectively. With these covariances and observations, the ensemble of Ku-band solutions can be updated using the EnKF,

$$\mathbf{X}_i' = \mathbf{X}_i + \mathbf{PH^T}\left(\mathbf{HPH^T} + \mathbf{R}\right)^{-1}\left[\mathbf{Y} - \mathbf{H}\left(\mathbf{X}_i\right)\right], \tag{5}$$

where

$$\mathbf{PH^T} = \frac{1}{N-1}\sum_{i=1}^{N}\left(\mathbf{X}_i - \overline{\mathbf{X}}\right)\left[\mathbf{H}\left(\mathbf{X}_i\right) - \overline{\mathbf{H}(\mathbf{X})}\right]^T, \tag{6}$$

$$\mathbf{HPH^T} = \frac{1}{N-1}\sum_{i=1}^{N}\left[\mathbf{H}\left(\mathbf{X}_i\right) - \overline{\mathbf{H}(\mathbf{X})}\right]\left[\mathbf{H}\left(\mathbf{X}_i\right) - \overline{\mathbf{H}(\mathbf{X})}\right]^T, \tag{7}$$

and

$$\mathbf{R} = \begin{bmatrix} \mathbf{W}_{\mathbf{Z_{Ka}}} & \mathbf{0} \\ \mathbf{0} & \mathbf{W}_{\mathbf{PIA}} \end{bmatrix}. \tag{8}$$

Here, $\mathbf{X}_i = [\ \mathbf{q}_{vi}\ \ \mathbf{q}_{cldi}\ \ \mathbf{ln(N}_{wi}\mathbf{)}\ ]^T$ is a vector of unknown parameters in the *i*th ensemble member, $\mathbf{Y} = [\mathbf{Z_{Ka}}\ \ \mathbf{PIA}]^T$ is a vector of observed Ka-band reflectivities and path-integrated attenuations, $\mathbf{PIA} = [\mathrm{PIA_{Ku}}\ \ \mathrm{PIA_{Ka}}]^T$, derived from the surface reference technique, $\mathbf{H}(\mathbf{X}_i)$ is the simulation of the observations $\mathbf{Y}$ from the unknown parameters of the *i*th ensemble member, $\mathbf{PH^T}$ is the ensemble covariance of the unknown parameters and the simulated observations, $\mathbf{HPH^T}$ is the ensemble covariance of the simulated observations, $\mathbf{R}$ is a matrix of the uncertainties in the observations, and N is the number of ensemble members. Estimated PIA's from the surface reference technique are provided by the Level 2 Radar Algorithm output.

The form of (5)-(8) is similar to Eqs. (8)-(11) in Grecu and Olson (2008), but applied to the dual-wavelength radar precipitation estimation problem described in Grecu et al. (2011). The objective is to modify the environmental and precipitation profile parameters from the Ku-band solution to the extent that the Ka band reflectivities and observed PIA's contain additional information. If the Ka band reflectivities are not available or totally attenuated by heavy rain, or if the rainfall is light (Rayleigh regime, where $Z_{Ku} \approx Z_{Ka}$), then the Ku-band solution will not be modified by $\mathbf{Z_{Ka}}$, although the **PIA** data can still alter the solution.

Equation (5) is applied to all 50 ensemble member profiles at each DPR footprint location, creating an output ensemble of μ, N_w, and D_o profiles and environmental parameters that are consistent with the observed reflectivities and path-integrated attenuations at both Ku and Ka band. These ensembles are passed to the Radiometer Module (Fig. 2c). Recall that each ensemble member profile is actually part of a 3D

field that spans the swath segment, and so there is a 50-member ensemble of 3D environmental/precipitation parameter fields that are input to the Radiometer Module.

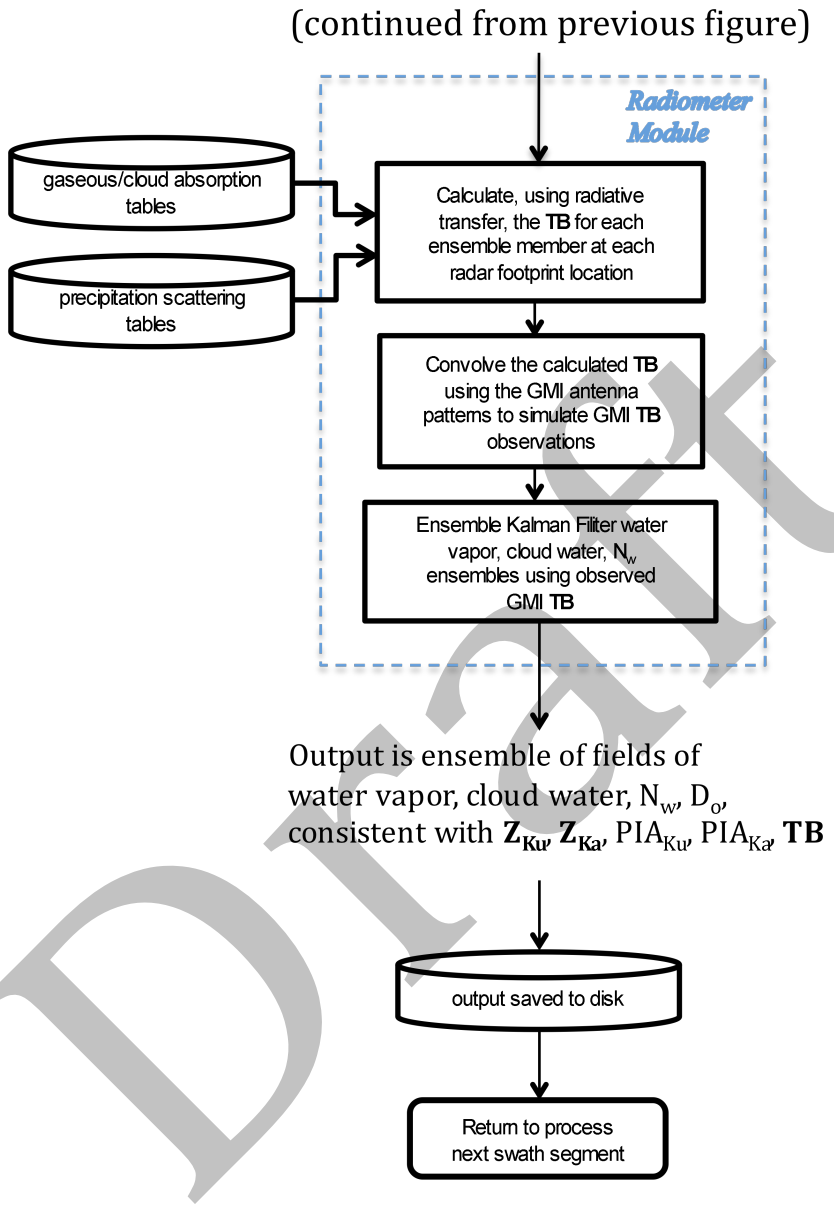

Fig. 2c. The Radiometer Module processing schematic of the Combined Radar-Radiometer Algorithm.

Now, considering only one ensemble member 3D field of environmental/ precipitation parameters, the single scattering properties at each radar bin location of the 3D field are calculated using the gaseous/cloud absorption and precipitation scattering tables previously described. Also, the surface emissivities at the GMI frequencies can be calculated from the *Tsfc* and *U10m* values that are also defined for that ensemble member. This is sufficient information to perform forward radiative

transfer calculations of the upwelling microwave brightness temperatures at the GMI channel frequencies and polarizations at the DPR footprint locations. The ensemble member is now associated with a 5 km (DPR) resolution field of computed upwelling radiances across the swath, and a convolution of this field by the GMI antenna patterns yields a simulation of the GMI brightness temperatures at the DPR footprint locations. The brightness temperature computations and antenna pattern convolutions are repeated for all of the ensemble member fields.

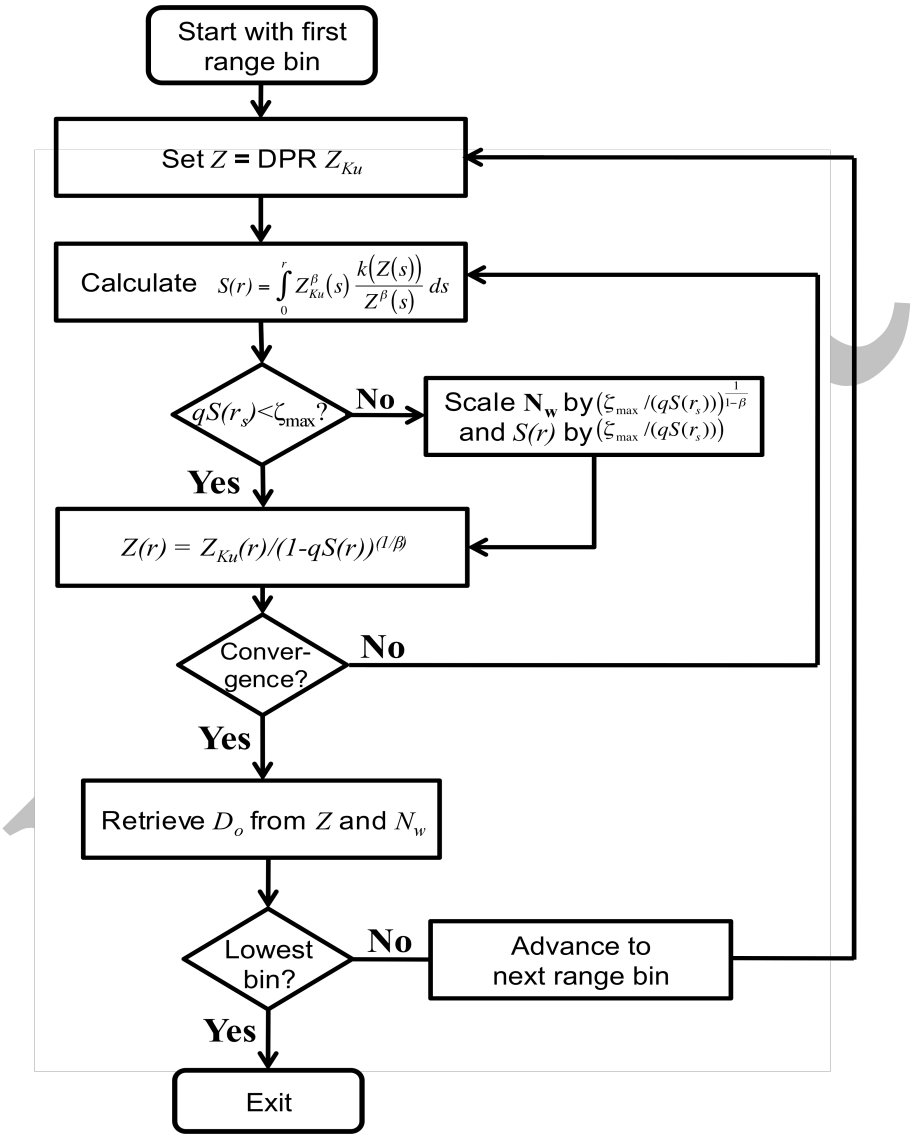

Fig. 2d. Schematic for the generalized Hitschfeld-Bordan method, contained in the Radar Module (see Fig. 2b).

At this stage, ensemble member fields of environmental/precipitation parameters, as well as consistent simulations of upwelling brightness temperatures at the GMI channel frequencies and polarizations have been created. Since coincident,

interpolated GMI brightness temperature observations are also available at the DPR footprint locations, ensemble covariances of the environmental/precipitation parameters and associated simulated brightness temperatures can be used to do an Ensemble Kalman Filtering of the environmental/precipitation parameters. However, the GMI antenna patterns may encompass many radar-derived precipitation profiles on the relatively fine-resolution DPR grid, and so the region of influence for the EnKF update must be specified. In the current implementation, the interpolated GMI brightness temperatures at a given DPR footprint location are used to drive the Kalman update of *only* the environmental/precipitation parameter ensemble at that location. The environmental/precipitation parameter ensembles associated with neighboring DPR footprints are not modified. In other words, only the environmental/precipitation parameters coinciding with the maximum of the GMI antenna pattern (or sensor response) are updated using the EnKF.

Therefore, at each DPR footprint location and for each ensemble member,

$$\mathbf{X}_i' = \mathbf{X}_i + \mathbf{P}\mathbf{A}^{\mathbf{T}}\left(\mathbf{A}\mathbf{P}\mathbf{A}^{\mathbf{T}} + \mathbf{W}_{\mathbf{TB}}\right)^{-1}\left[\mathbf{TB}_{\mathbf{obs}} - \mathbf{A}\left(\mathbf{X}_i^*\right)\right], \quad (9)$$

where

$$\mathbf{P}\mathbf{A}^{\mathbf{T}} = \frac{1}{N-1}\sum_{i=1}^{N}\left(\mathbf{X}_i - \overline{\mathbf{X}}\right)\left[\mathbf{A}\left(\mathbf{X}_i^*\right) - \overline{\mathbf{A}\left(\mathbf{X}^*\right)}\right]^T, \quad (10)$$

and

$$\mathbf{A}\mathbf{P}\mathbf{A}^{\mathbf{T}} = \frac{1}{N-1}\sum_{i=1}^{N}\left[\mathbf{A}\left(\mathbf{X}_i^*\right) - \overline{\mathbf{A}\left(\mathbf{X}^*\right)}\right]\left[\mathbf{A}\left(\mathbf{X}_i^*\right) - \overline{\mathbf{A}\left(\mathbf{X}^*\right)}\right]^T. \quad (11)$$

Note that (9)-(11) have the same form as (5)-(7), but here, $\mathbf{TB_{obs}}$ is the set of interpolated, observed brightness temperatures from GMI, $\mathbf{A}(\mathbf{X}_i^*)$ is the set of simulated GMI brightness temperatures derived from the field of environmental/precipitation parameters $\mathbf{X}_i^*$ of the *i*th ensemble member, $\mathbf{PA^T}$ is the covariance of environmental/precipitation parameters and simulated brightness temperatures, $\mathbf{APA^T}$ is the covariance of the simulated brightness temperatures, and $\mathbf{W_{TB}}$ is the covariance of noise in the observed brightness temperatures. Note that as in (5), only the environmental/precipitation parameter vector associated with the vertical profile, $\mathbf{X}_i = [\ \mathbf{q}_{vi}\ \ \mathbf{q}_{cldi}\ \ \mathbf{ln(N_{wi})}\ ]^T$, is updated, while the 3D field, $\mathbf{X}_i^*$, of environmental/precipitation parameters is used to simulate the GMI brightness temperatures.

Using (9), the ensembles of environmental/precipitation parameters are updated sequentially over the portions of the swath where precipitation is detected. However, for the purpose of computational efficiency the right-hand side of (9) is not updated as the $\mathbf{X}_i$ are updated, and within the operational constraints of NASA's Precipitation Processing System (PPS), the GPM Combined Algorithm can be considered a one-pass method.

The outputs of the Radiometer Module are ensembles of environmental/ precipitation parameters consistent with both the DPR and GMI observations and their errors. The best estimate of the environmental/precipitation parameters at any DPR location is given by the mean of the ensemble,

$$\overline{\mathbf{X}} = \frac{1}{N}\sum_{i=1}^{N}\mathbf{X}_i \ , \tag{12}$$

and the uncertainty of the best estimate is given by the ensemble standard deviation,

$$\mathbf{s}_{\mathbf{X}} = \left[\frac{1}{N-1}\sum_{i=1}^{N}\left(\mathbf{X}_i - \overline{\mathbf{X}}\right)\left(\mathbf{X}_i - \overline{\mathbf{X}}\right)^T\right]^{1/2} . \tag{13}$$

The uncertainty, $\mathbf{s}_{\mathbf{X}}$, represents the error in the best estimate due to errors in the observations as well as ambiguities due to the limited information content of the observations. Note that other precipitation-related parameters, such as the surface rainfall rate or precipitation liquid water content can be estimated using (5), (9), (12), and (13), by adding these to the vector $\mathbf{X}_i$.

Once the output of the Radiometer Module is saved to disk, the next 300 scan lines of DPR and coincident GMI data are processed, and so on, until the whole orbit is processed.

In the following subsections, the basic functions of the three primary modules of the Combined Radar-Radiometer Algorithm, including input and output parameters, are described. Supporting modules, datasets, and tables are described in section 4.

Environment Module

The basic function of the Environment Module is to ingest one orbit of DPR reflectivities, as well as an orbit of GMI brightness temperatures, and produce fields of environmental (non-precipitation) parameters at DPR sampling resolution. The sensor inputs required are the calibrated DPR Z_{Ku} and Z_{Ka} profiles from the Level 2 Radar Algorithm, and the intercalibrated GMI brightness temperatures from the Level 1C Radiometer Algorithm. One orbit of input data from each of these algorithms is required, but in addition, two 50-scan overlap fields of GMI data at the orbit boundaries is needed.

In addition to these sensor inputs, the Environment Module requires Level 2 Radar Algorithm ancillary environmental data that include pressure, temperature, vapor density, cloud liquid water content, surface skin temperature, and wind speed at 10-m altitude, interpolated to the DPR footprint locations and range bin altitudes, as appropriate. These data are provided by the Vertical Profile Submodule (VER) of the Radar Algorithm, which interpolates the Japanese Meteorological Agency's (JMA) analyses and forecasts to the DPR locations/range bins; see section 4 for details. The analysis fields of total precipitable water, TPW_{anal}, non-precipitating cloud liquid

water path, $CLWP_{anal}$, surface skin temperature, $Tsfc_{anal}$, and 10-m altitude wind speed, $U10m_{anal}$ are used to constrain Bayesian estimates of these environmental parameters; see (1). The Environment Module also requires input from a static geographic database that includes surface water coverage and elevation information; see section 4.

The Bayesian estimator of environmental parameters in the Environment Module requires supporting data that describe the relationships between the environmental parameters and upwelling microwave brightness temperatures at the GMI channel frequencies/polarizations. These relationships are represented by large databases of environmental parameters and physically-consistent microwave brightness temperatures. A database relating environmental *TPW*, *CLWP*, *Tsfc*, and *U10m* to microwave brightness temperatures over ocean backgrounds has been developed, and so currently, estimates of these environmental parameters are performed only over open ocean regions. The Bayesian estimator will be extended to over-land applications by including over-land distributions of environmental parameters and physically-consistent microwave brightness temperatures in the supporting database; see section 4 for details.

The output of the Environment Module are estimates of *TPW*, *CLWP*, *Tsfc*, and *U10m*, that are interpolated into precipitation regions to create a complete field of environmental parameters across the Ku band swath.

Radar Module

The Radar Module accepts input fields of environmental parameters from the Environment Module as well as DPR reflectivity and path-integrated attenuation information. Its primary function is to estimate ensembles of environmental and precipitation parameters consistent with these input data at each DPR footprint location, using an Ensemble Kalman Filtering (EnKF) approach. Specifically, input to the Radar Module are fields of environmental *TPW*, *CLWP*, *Tsfc*, and *U10m* from the Environment Module, as well as calibrated Z_{Ku} and Z_{Ka} profiles from the Level 2 Radar Algorithm, passed through the Environment Module. Other inputs from the Level 2 Radar Algorithm are precipitation detection and classification information that establish the basic *a priori* vertical structure of the precipitation where it is detected. Precipitation detection data are derived from the Preparation Submodule (PRE) of the Radar Algorithm, while classification information is derived from the Classification Submodule (CSF) of that algorithm. In addition, estimates of path-integrated attenuation at Ku and Ka band, symbolized by PIA_{Ku} and PIA_{Ka}, respectively, are input from the Radar Algorithm's Surface Reference Technique Submodule (SRT).

The Radar Module also draws upon tabulated gaseous/cloud absorption coefficients and single-scattering parameters that have been pre-computed for the purpose of algorithm computational efficiency. Tables of gaseous absorption coefficients at Ku and Ka band, as well as the GMI channel frequencies, are currently calculated as functions of pressure, temperature, and vapor density. Tables of cloud

water/ice absorption coefficients at the same frequencies are currently calculated as functions of temperature and equivalent liquid water content; see section 4 for details.

Because precipitation of all phases produces scattering as well as absorption/emission of microwaves, and since the particle size distribution, phase, and temperature of precipitation determine its bulk scattering and absorption/emission characteristics, separate databases are used to tabulate the single-scattering properties of precipitation. In these tables, values of reflectivity, extinction coefficient, scattering coefficient, and asymmetry parameter are tabulated as functions of μ, D_o, and $\ln(N_w)$, which define a normalized gamma distribution of precipitation particle sizes. Ice, liquid water, and mixed-phase particles are represented in the tables. Using the tables, the scattering parameters are derived at Ku and Ka band in the Radar Module.

The output of the Radar Module are ensembles of 3D fields of pressure, temperature, humidity, cloud water content, μ, N_w, and D_o, and 2D fields of *Tsfc* and *U10m*, consistent with the DPR fields of Z_{Ku}, Z_{Ka}, PIA_{Ku}, PIA_{Ka}, and their uncertainties.

Radiometer Module

The Radiometer Module accepts input ensemble fields of environmental/ precipitation parameters from the Radar Module as well as GMI brightness temperatures passed through the Radar Module. Its primary function is to create ensembles of environmental/precipitation parameters consistent with these input data at each DPR footprint location, using an EnKF approach. Specifically, ensembles of 3D fields of pressure, temperature, humidity, cloud water content, *Tsfc*, *U10m*, μ, N_w, *and* D_o, as well as 2D fields of *Tsfc* and *U10m*, are input to the Radiometer Module. Intercalibrated GMI brightness temperatures from the Level 1C Radiometer Algorithm are also input.

In addition to the inputs from the Radar Module, the Radiometer Module utilizes the static gaseous/cloud absorption and scattering tables described in the previous subsection. Based upon the input ensembles of pressure, temperature, water vapor, cloud water, μ, N_w, and D_o fields, the Radiometer Module derives the corresponding fields of single-scattering parameters for each ensemble member at the GMI channel frequencies using these tables. In addition, the fields of *Tsfc* and *U10m* associated with the ensembles are used to calculate the ocean surface emissivity, based upon the FASTEM4 model; see Liu et al. (2011). Currently over other surfaces, only DPR-derived information is used in the Combined Algorithm, and so surface emissivities are not calculated. Our plan is to estimate the emissivities of these other surfaces using the TELSEM tool in conjunction with analysis data (to provide *a priori* information); see section 4.

The atmospheric temperature and single-scattering properties, as well as the surface skin temperature and emissivities, at each DPR footprint location are input to a radiative transfer model to calculate the upwelling microwave brightness

temperatures at that location. Eddington's Second Approximation, which accounts for multiple-scattering effects but which is also computationally-efficient, is utilized for these calculations; see Kummerow 1993; Olson et al. 2001.

The output of the Radiometer Module are 3D ensemble fields of pressure, temperature, humidity, cloud water content, μ, N_w, and D_o, and 2D ensembles of *Tsfc* and *U10m*, consistent with the DPR fields of Z_{Ku}, Z_{Ka}, PIA_{Ku}, PIA_{Ka}, as well as the fields of GMI *TB*'s and their uncertainties.

4. Ancillary Datasets

In the current algorithm formulation, only the Analysis Data, described below, must be ingested from an external source during Combined Algorithm processing. The other databases and tables are static and will be read into memory upon the execution of the algorithm software.

Geographic Data

A geographic database containing water coverage and elevation information at 5 km resolution is required by the Environment Module; see section 3. Water fractions in the database are derived from the Moderate Resolution Imaging Spectroradiometer (MODIS) 250 m resolution land-water mask, and elevations are derived from the Shuttle Radar Topography Mission 30" (SRTM30) data, both re-projected to the NASA Land Information System (LIS) 1 km grid. Finally, the 1 km resolution data are averaged to 5 km to match the resolution of the DPR.

Analysis Data

Analysis data are required to produce initial estimates of environmental parameters such as total precipitable water, TPW_{anal}, cloud liquid water path, $CLWP_{anal}$, surface skin temperature, $Tsfc_{anal}$, and 10-m altitude wind speed, $U10m_{anal}$; see (1) in section 3. The current algorithm design requires space-time interpolation of these data from the Japanese Meteorological Agency's (JMA) global analyses (GANAL) during standard algorithm processing. The data are interpolated to the DPR footprint/range bin locations and overpass times in the Vertical Profile Submodule (VER) of the Level 2 Radar Algorithm and then output. For near real-time processing, the JMA analysis is supplemented with JMA forecast fields, but if these fields are not received in time for any reason, Japanese 25-year Re-analysis (JRA-25) data are substituted for the JMA analysis/forecast data in the VER processing.

Databases Supporting Bayesian Estimation of Environmental Parameters

The Bayesian estimator, (1), of environmental parameters requires supporting data that represent the relationships between the environmental parameters and upwelling microwave brightness temperatures at the GMI channel frequencies/ polarizations; see section 3. Currently, estimates of the environmental parameters *TPW*, *CLWP, Tsfc,* and *U10m* are performed only over open ocean regions. Therefore, the database that supports the Bayesian estimation of these parameters

contains large, *a priori* distributions of *TPW*, *CLWP, Tsfc,* and *U10m* and associated upwelling brightness temperatures at the GMI channel frequencies/polarizations. The environmental parameter distributions of the supporting database are derived from SSM/I retrievals; then the parameters are used to construct simple vertical profiles of temperature, water vapor, and cloud water. The microwave absorption properties of atmospheric gases and cloud liquid water are derived from the microwave single-scattering tables described below. Surface microwave emissivities as functions of *Tsfc*, *U10m*, and salinity are given by the FASTEM4 model (Liu et al. 2011), with salinity derived from the NOAA/NODC World Ocean Atlas 2009; see Antonov et al. 2010. Finally, radiative transfer calculations of upwelling brightness temperatures corresponding to the environmental conditions are performed using Eddington's Second Approximation for an assumed plane-parallel atmosphere; see Kummerow 1993; Olson et al. 2001.

The current algorithm does not utilize radiometer data over surfaces other than open ocean. Our plan is to estimate land surface emissivities using brightness temperature data from the GMI in conjunction with the JMA analysis data. This will require extending the Bayesian estimator to land surfaces by replacing *U10m* in (1), above, with parameters that are statistically related to the surface emissivity. The statistical parameters can be derived from the Tool to Estimate Land Surface Emissivities in the Microwave (TELSEM) software; see Aires et al. (2010). TELSEM is a program that allows the user to interpolate an atlas of land surface emissivities and their interchannel covariances to the GMI channel frequencies/polarizations and viewing angle. The atlas is drawn from a 16-year, quarter-degree resolution dataset of emissivities based upon cloud-cleared SSM/I observations; see Prigent et al. (2006). Shown in Fig. 3 are global distributions of TELSEM-derived mean emissivities and emissivity standard deviations drawn from the corresponding TELSEM covariance matrices.

Filipe Aires (personal communication) has identified ten land surface regimes for which the emissivities/covariances are self-similar, and so the regime-dependent mean emissivities and their covariances can be computed. It follows that a multichannel eigenvector representation of the emissivities in each regime can also be derived. Our work has shown that for most land surfaces, the weighting of one or two emissivity eigenvectors can well represent most of the multichannel variability of surface emissivities. Therefore, *U10m* can be replaced by eigenvector weights in (1) to estimate the environmental parameters over land, if there is sufficient information in the atmospheric analysis to constrain the atmospheric parameters. An alternative, direct estimator of emissivity using analysis information has been developed by Masunaga and Furuzawa (personal communication). These estimators will be tested in the near term to determine their utility in deducing the environmental parameters over land surfaces.

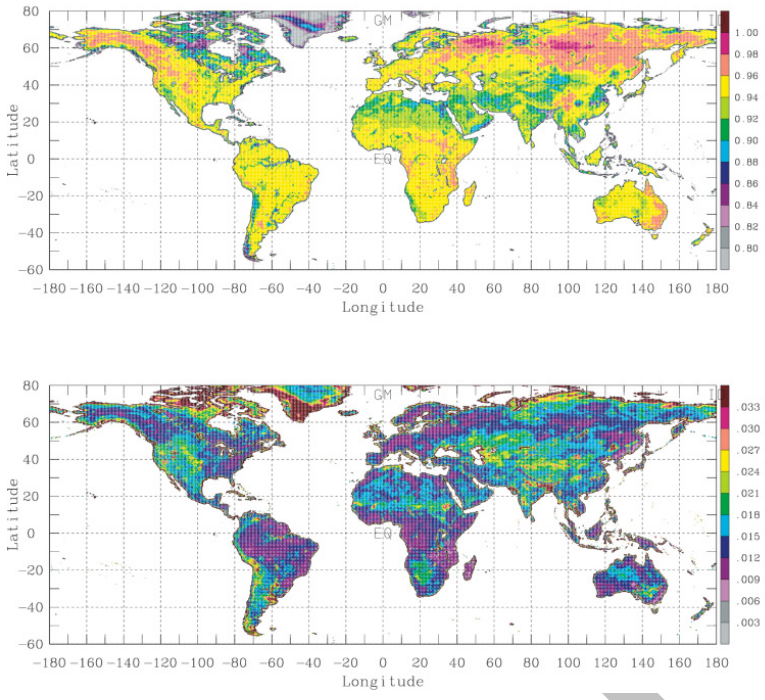

Fig. 3. TELSEM mean emissivity estimates at 31.4 GHz (top), together with the corresponding emissivity standard deviations (bottom) from the TELSEM covariance matrices.

Microwave Absorption and Single-Scattering Tables

Two types of tables are produced by the GPM Radar Algorithm and Combined Algorithm Teams. The first table type contains microwave absorption coefficients for atmospheric gaseous constituents indexed by pressure, temperature, and humidity, and also cloud water/ice absorption coefficients indexed by temperature and liquid-equivalent cloud water content. Tables of gaseous absorption coefficients at Ku and Ka band, as well as the GMI channel frequencies, are currently calculated as functions of pressure, temperature, and vapor density using the Millimeter-wave Propagation Model 1993 (see Liebe, 1989; Liebe et al. 1992). Tables of cloud water/ice absorption coefficients at the same frequencies are currently calculated as functions of temperature and equivalent liquid water content using Rayleigh theory.

Because precipitation of all phases induces scattering as well as absorption/emission of microwaves, and since the particle size distribution, phase, and temperature of precipitation determine its bulk (size distribution integrated) scattering and absorption/emission characteristics, separate tables are used to store the single-scattering properties of precipitation. This second table type contains bulk reflectivities, extinction coefficients, scattering coefficients, and asymmetry parameters of precipitation at Ku and Ka band, as well as the GMI channel frequencies. These bulk scattering parameters are integrated over an assumed gamma distribution and indexed by μ, N_w, and D_o, which define the normalized gamma distribution. Separate tables are generated for liquid and ice-phase precipitation at

different temperatures; for mixed-phase precipitation, tables are created for different displacements relative to the freezing level. All particles are currently assumed to be spherical, homogeneous mixtures of ice, air, and liquid water, with different fractions of each depending on the precipitation phase.

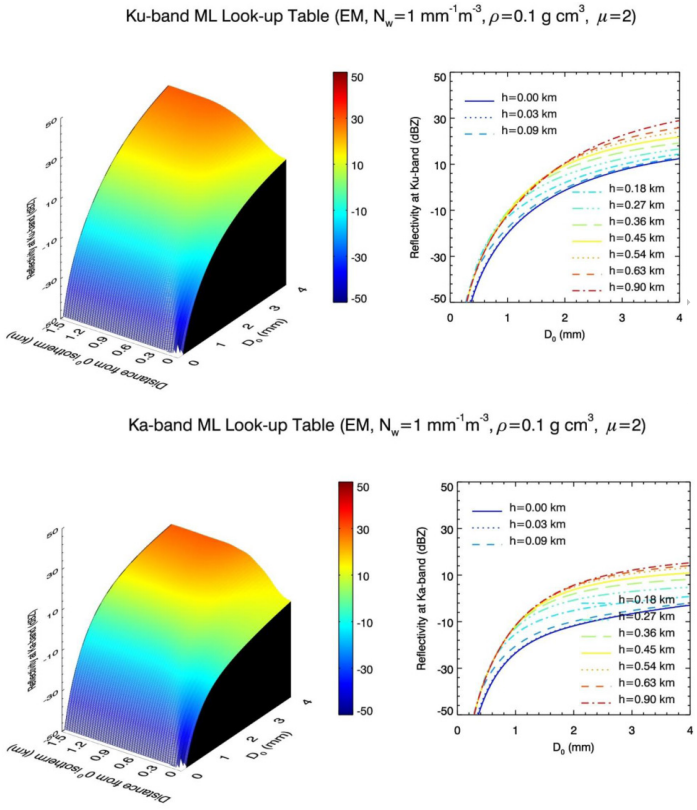

Fig. 4. Graphical illustrations of Ku-band (top) and Ka-band (bottom) scattering table entries for radar reflectivities within the melting layer. Color plots show the variation of reflectivity (given N_w) with both D_o and distance below the 0°C level. Line plots show the same information for specific depths below the 0°C level.

A graphical illustration of entries in the second table type is shown in Fig. 4 for Ku and Ka band reflectivities of melting snow particle distributions at various depths below the freezing level. The initial snow particles and partially melted particles are assumed to be spherical, homogeneous ice-air or ice-air-liquid mixtures. Anticipated particle modeling improvements will include non-spherical melting snow, but the form of the tables will remain essentially unchanged, facilitating comparisons of different particle models on Combined Algorithm performance.

5. Summary of Algorithm Input/Output

Input to the Combined Algorithm is derived from Level 2 Radar Algorithm (2AKu, 2AKuENV, 2ADPR, 2ADPRENV) products and from the Level 1C

Radiometer Algorithm GMI (1CGMI) product, as well as the ancillary datasets described in section 4.

The output of the Combined Algorithm is the 2BCMB product, which contains two swaths of data. Precipitation estimates in the S1 output swath are derived from coincident DPR Ku band reflectivities/PIA's and GMI brightness temperatures, and these estimates will extend across the entire Ku band swath. Precipitation estimates in the S2 output swath are derived from coincident DPR Ku and Ka band reflectivities/PIA's and GMI brightness temperatures. The S2 precipitation estimates are therefore limited to the DPR Ku-Ka overlap swath. Since the S2 swath estimates draw upon the maximum amount of information from the GPM Core sensors, these estimates will be the main tool for cross-calibrating the GPM constellation radiometer precipitation estimates through the creation of *a priori* databases. The same Combined Algorithm software architecture is used to create either the S1 or S2 output swaths.

A complete listing of Combined Algorithm input/output parameters is included in Appendix A. Output volumes and algorithm processing requirements are included in Appendix B and C, respectively.

6. Algorithm Testing Plan

Prior to the GPM Core Observatory launch, testing of the Combined Algorithm or Algorithm components will fall into three categories: Sensitivity Testing, Physics Testing, and Pre-launch Validation. After GPM Core launch, Sensitivity Testing and Physics Testing will continue, and Pre-launch Validation activities will evolve into Post-launch Validation.

Sensitivity Testing

Sensitivity tests basically quantify the impact of different algorithm modifications on output products. So, it is possible that even if the Combined Algorithm investigators suspect that a particular algorithm modification should have a significant impact based upon previous work or intuitive reasoning, that modification may actually have little impact or an impact that was not foreseen. Sensitivity testing can therefore be used to prioritize or re-focus areas of algorithm development based upon the specific impact algorithm modifications have on output.

Input data for sensitivity testing can vary depending on the algorithm modification. Typically, we will use Ku band radar data from either airborne sensors or TRMM observations to synthesize Ka band radar reflectivity and GMI brightness temperature observations. In this way we can ensure physical consistency between the radar and radiometer channels using the same forward modeling assumptions. The following are some ongoing and planned areas of sensitivity testing:

- impact of changes in algorithm methodology
- impact of different input data (e.g., radar vs. radar-radiometer)

- impact of PSD description
- impact of assumed environmental/precipitation parameter correlations
- impact of particle scattering assumptions
- impact of precipitation phase transition assumptions
- impact of land surface characterization and physical parameterizations
- impact of source of ancillary (analysis) data
- impact of radar non-uniform beamfilling assumptions

This list is by no means exhaustive.

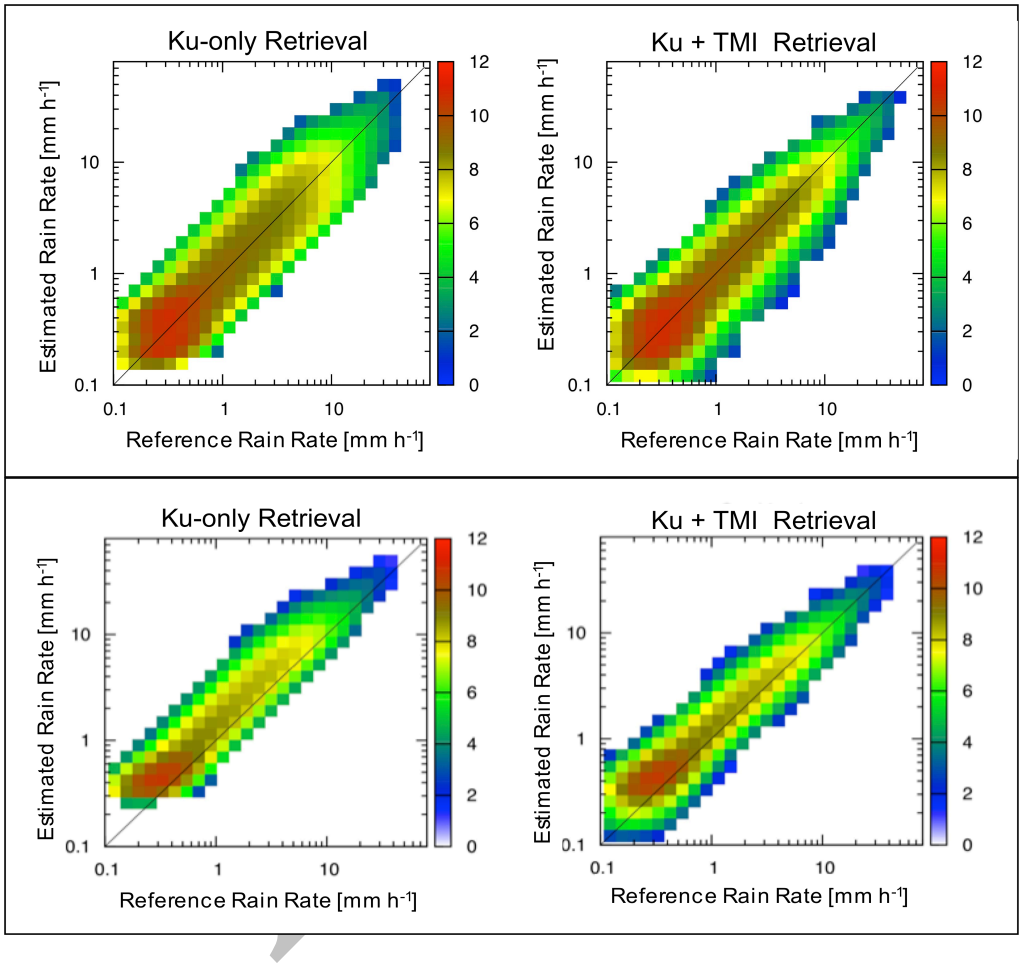

Fig. 5. Shown in the top panels are 2D histograms of synthetic retrievals of surface rain rate vs. reference rain rates, using only Ku band input data (left panel) and using both Ku band and TMI input data (right panel). The bottom panels are the same, except that the mean of the initial guess N_w values is assumed to be 4x the mean of the actual reference values.

An example of sensitivity testing is the study of the impact of DPR and GMI input data on Combined Algorithm estimates relative to estimates based upon the DPR input data alone. Shown in Fig. 5 are 2D histograms (similar to scatterplots) of estimated surface rainfall rates from algorithm applications to synthetic data versus

the known reference rainfall rates. Only the Ku band reflectivity data are utilized in the algorithm applications illustrated on the left-hand side of the figure, while both Ku band and TMI brightness temperature data are utilized in the algorithm applications illustrated on the right-hand side. If the initial guess ensemble of N_w values has the same mean as the reference values, then the addition of the TMI observations reduces the scatter of estimated rainfall rates relative to the reference values. If the initial guess ensemble of N_w values is biased by a factor of 4 relative to the reference values, there is a greater bias correction if both the Ku band and TMI observations are utilized.

Sensitivity testing is expected to be a long-term activity, extending past the GPM Core launch, which will help us to improve our understanding of the Combined Algorithm's response to a variety of potential modifications.

Physics Testing

The objective of Physics Testing is to verify assumptions in the forward models that relate environmental/precipitation parameters to sensor observations. Since the current TRMM and GPM radars and radiometers have relatively low resolution, field campaign observations from airborne and ground-based instrumentation generally provide superior data for physics testing. These data may include remote sensing radar and radiometer observations as well as *in situ* measurements.

Ongoing or planned areas of physics testing include

- assessment of appropriate physical models for ice-phase precipitation
- assessment of proper parameterizations for the ice-to-liquid phase transition
- assessment of appropriate physical models for mixed-phase precipitation
- assessment of physical models for land surface emissivities

Fig. 6 illustrates a precursor of physics testing to determine appropriate physical parameterizations of ice-phase precipitation in the Combined Algorithm. In this test, different physical models are assumed for describing the single-scattering properties of ice-phase precipitation in a precipitation estimation algorithm. The estimation algorithm is applied to Dual-frequency Airborne Precipitation Radar (APR-2) Ku and Ka band observations from the Genesis and Rapid Intensification Processes (GRIP) field campaign. The reflectivity observations (not shown) indicate a stratiform precipitation region with embedded convective elements. It is evident from the figure that the choice of ice-phase precipitation scattering model has an impact on the estimation of the precipitation mass-weighted particle diameter, water content, and rainfall rate.

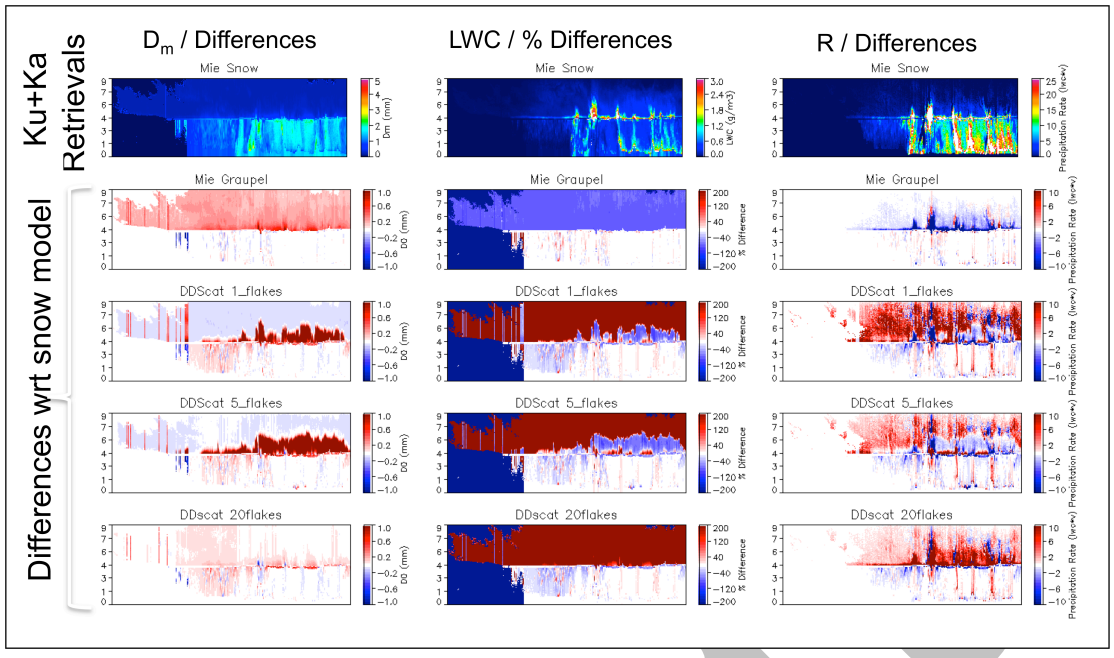

Fig. 6. Top row are estimated mass-weighted mean diameter, D_M (similar to D_o), liquid water content, LWC, and rain rate, R, based upon airborne APR-2 Ku and Ka band radar data. Ice-phase precipitation is assumed to be spherical snow particles with mixed ice-air dielectric properties. Shown in the second row are the differences between Ku/Ka band estimates assuming spherical, mixed-dielectric graupel particles and mixed-dielectric snow particles. Shown in the third, fourth, and fifth rows are the differences between estimates assuming structured snow particles composed of multiple dendritic flakes and spherical mixed-dielectric snow particles.

During the Midlatitude Continental Convective Clouds Experiment (MC3E) field campaign (and upcoming GPM Cold-season Precipitation Experiment [GCPEX] field campaign), airborne dual-frequency radar observations are coupled with coincident microwave brightness temperature measurements and *in situ* microphysics probe observations of precipitation. The precipitation algorithm will be applied to these combined radar-radiometer data to see if reasonable fits to the data can be achieved, and to see if agreement with *in situ* observations is possible, given different assumed ice scattering parameterizations.

Physics testing is expected to be a long-term activity, extending past the GPM Core launch, that will help us improve our understanding of the Combined Algorithm's forward model and its uncertainties.

Pre-launch Validation

Prior to the GPM Core Observatory launch, the Combined Algorithm will be examined to determine (a) in TRMM applications, how Combined Algorithm precipitation estimates compare to TRMM V7 Algorithm estimates and well-calibrated ground-based radar estimates, and (b) whether or not Combined Algorithm

estimates are expected to meet the GPM Level-1 Science Requirements. It is stated in the Science Requirements that the algorithm should be capable of estimating instantaneous surface rainfall rates at 50 km resolution with a bias and random error within 50% at 1 mm h^{-1} rain rate and within 25% at 10 mm h^{-1} rain rate.

With respect to TRMM applications, the Combined Algorithm performance should be similar to what might be expected outside the GPM Ka band swath, where only Ku band and GMI brightness temperature observations will be available. Shown in Fig. 7 are preliminary comparisons of surface rain rate estimates from the TRMM V7 Radar Algorithm (2A25), the TRMM V7 Combined Algorithm (2B31), and the GPM prototype Combined Algorithm (EnKF). Note the general similarity between the rain rate estimates, which is attributed to the similar physical basis of all three algorithms.

Although coincident ground-based radar observations are not available for the precipitation systems shown in Fig. 7, well calibrated radar with raingages sited within the radar observing domain are available from the Melbourne, Florida and Kwajalein Atoll, Republic of Marshall Islands ground validation cites; see Wolff et al. (2005). Both sites feature S-band, nearly non-attenuating radars; the KPOL radar at Kwajalein is polarimetric and the Melbourne WSR-88D radar will be upgraded to polarimetric in January, 2012. Polarimetric capability will help improve quality control of the data and provide more definitive rain rate estimates. These high quality ground validation estimates will be compared to Combined Algorithm estimates to providing evidence for whether or not the Science Requirements will be met by the algorithm.

In addition, the GPM Validation Network (VN) and National Mosaic & Multi-Sensor Quantitative Precipitation Estimation product (NMQ) called Q2, will provide large-scale coverage of three dimension reflectivity distributions and surface rainfall rates, respectively, for identifying locally large discrepancies between satellite and ground-based measurements. Both products are based upon the US WSR-88D radar network. The VN network covers the southeast US within the TRMM range of observations, providing geometrically "matched" reflectivity data from the network and the TRMM PR; see Schwaller and Morris (2011). Processing of TRMM estimates from the prototype Combined Algorithm in the same way will facilitate similar intercomparisons. Of particular interest is how well the attenuation corrected reflectivities from the Combined Algorithm agree with the VN S-band reflectivities, that are essentially unaffected by attenuation. To do these intercomparisons properly, a small Mie correction should be applied to the Combined estimates of attenuation-corrected Ku band reflectivities; see Liao and Meneghini (2009). The NOAA Q2 product is a 1 km, 5 minute resolution instantaneous rain rate product derived from the National Weather Service NEXRAD radar network and coincident raingages; see Vasiloff et al. (2007); Amitai et al. (2009). Like the VN, the Q2 data have the advantage of broad spatial coverage, with observations extending over the continental US starting in 2006.

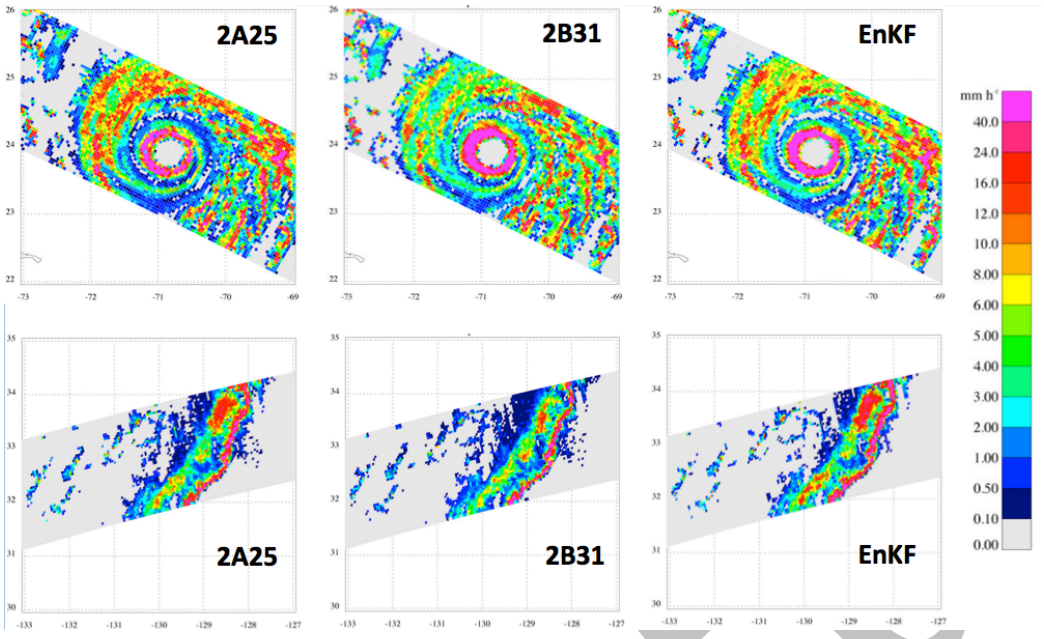

Fig. 7 Top row, estimated surface rainfall rates in Tropical Cyclone Floyd at 09 UTC 13 September 1999 from the TRMM V7 2A25 (radar-only), TRMM V7 2B31 (radar-radiometer) and TRMM EnKF (prototype GPM radar-radiometer) algorithms. Bottom row, same as top row but TRMM estimates are for a wintertime cold frontal band over the Eastern Pacific Ocean at 00 UTC 19 February 2001.

In addition to the evaluation of Combined Algorithm estimates using TRMM data, the full algorithm implemented at the PPS will be tested with synthetic input data derived from Cloud-System Resolving Models (CSRM's). Table 1 indicates CSRM simulations that have been performed to serve as a testbed for prototype GPM algorithms. These simulations correspond to recent field campaign observing periods and cover a broad range of climatic regimes and precipitation systems types. Field observations from aircraft and ground-based radars, disdrometers, etc., that were deployed during these campaigns will be used to help validate the structure and microphysics of the simulated precipitation.

Table 1. Listing of CSRM simulations that will provide a testbed for synthetic retrieval tests in the Pre-launch era.

Campaign	Case & Date	Details
C3VP (Canada)	Lake effect 1/19/2007	Lake effect snow extended from Great Lakes. Narrow and shallow, but robust snow band.
	Synoptic 1/21/2007	Large-scale, relatively spatially homogeneous snow fall event.
LPVEx (Finland)	High 0°C Level 9/21/2010	Large-scale, mixed-phase stratiform rain with relatively high (~2400m) altitude of melting band.

LPVEx (Finland)	Low 0°C Level 10/20/2010	Large-scale, mixed-phase stratiform rain with low (~1000m) altitude of melting band.
MC3E (Oklahoma)	Squall line 4/25/2011	Multi-cell MCS and stratiform rain.
	Squall Line 5/20/2011	Severe convection, severe t-storm with trailing stratiform rain.
TWP-ICE (Darwin)	Cumulus Congestus 1/19/2007	Shallow cumulus congestus
	MCS 1/21/2007	Propagating MCS

Radar reflectivities and *PIA*'s at Ku and Ka band and brightness temperatures at the GMI channel frequencies and polarizations are simulated from the CSRM microphysics fields. The single-scattering properties of precipitation and radiative transfer are computed as they are in the forward radiative model of the Combined Algorithm. The simulated DPR and GMI data are then put in the same file formats as the Level 1 data at PPS. The objective is to mimic the inputs to the algorithm for the purpose of testing both the basic function of the algorithm within the PPS environment as well as the credibility of algorithm-estimated precipitation fields. Regarding the latter, the precipitation fields of the CSRM testbed provide a reference, or "truth", against which algorithm estimates may be directly compared. The bias and random error of algorithm estimates will then be evaluated with respect to the Science Requirements to judge the potential of the algorithm to meet those Requirements.

Post-launch Validation

After the GPM Core Observatory launch and initial checkout period, ground validation of Combined Algorithm estimates of precipitation will continue using data from the radar sites at Melbourne and Kwajalein. These data-intensive sites will be augmented with observations from NASA's NPOL radar and supporting raingage network at NASA Wallops Flight Facility, as well as higher-latitude sites in Finland, Canada, and S. Korea. Also, it is expected that by the time of GPM launch, the US National Radar Network will be completely upgraded to dual-polarization, leading to improved accuracy of quantitative precipitation estimates from the NMQ. It is anticipated that with the participation of Environment Canada, the NMQ network will be extended from the continental US into Canada. Validation strategies will be much the same as those used to evaluate TRMM-based algorithm estimates in the Pre-launch era; see the preceding subsection.

Metrics

As shown in Olson et al. (2006), the use of instantaneous, 50 km resolution rain rate estimates represents a reasonable compromise in resolution for evaluating algorithm errors. Although validation at resolutions down to 5 km (the nominal DPR resolution) may be attempted, the influence of satellite vs. ground radar collocation errors degrades any derived statistics. Accumulation of these estimates over seasons could reveal spatial patterns of bias (relative to reference estimates) that would be helpful for diagnosing systematic algorithm errors.

Standard bivariate statistics of the "errors" between Combined Algorithm rain estimates and ground-based estimates, such as the mean error (bias), error standard deviation, and correlation coefficient will be computed, generally stratified by the rain intensity. These statistics can be used to assess the algorithm's performance relative to the Level 1 Science Requirements, for example. However, information more relevant to algorithm improvement can be gained if the statistics are stratified by other variables that indicate specific state dependencies of the error. For example, are the errors functions of surface skin temperature, total precipitable water, or other variables that indicate the climate regime, or, are the errors functions of the precipitation system or type, such as the convective/stratiform class? Stratification of statistics to reveal state dependencies of algorithm error will be important for diagnosing algorithm deficiencies, especially in the early phases of the GPM Core mission.

In addition to meeting the L1 Science Requirements, a measure of the success of our effort will be the quantification of any improvements in combined radar-radiometer estimates relative to radar-only estimates within the GPM Combined Algorithm framework.

7. References

Aires, F., C. Prigent, F. Bernardo, C. Jimenez, R. Saunders, and P. Brunel, 2011: A Tool to Estimate Land Surface Emissivities in the Microwave (TELSEM) for use in numerical weather prediction. Q. J. R. Meteorol. Soc., **137**, 690-699.

Amitai, E., X. Llort, and D. Sempere-Torres, 2009: Comparison of TRMM radar rainfall estimates with NOAA next-generation QPE. *J. Met. Soc. Japan*, **87A**, 109-118.

Anderson, J. L., 2003: A local least squares framework for ensemble filtering. *Mon. Wea. Rev.*, **131**, 634-642.

Antonov, J. I., D. Seidov, T. P. Boyer, R. A. Locarnini, A. V. Mishonov, H. E. Garcia, O. K. Baranova, M. M. Zweng, and D. R. Johnson, 2010: *World Ocean Atlas 2009, Volume 2: Salinity.* S. Levitus, Ed. NOAA Atlas NESDIS 69, U.S. Government Printing Office, Washington, D.C., 184 pp.

Grecu, M., and W. S. Olson, 2008: Precipitating snow retrievals from combined airborne cloud radar and millimeter-wave radiometer observations. *J. Appl. Meteor. and Climatol.*, **47**, 1634-1650.

Grecu, M., L. Tian, W. S. Olson, and S. Tanelli, 2011: A robust dual-frequency radar profiling algorithm. *J. Appl. Meteor. and Climatol.*, **50**, 1543-1557.

Liao, L., and R. Meneghini, 2009: Changes in the TRMM Version-5 and Version-6 Precipitation Radar products due to orbit boost. *J. Met. Soc. Japan*, **87A**, 93-107.

Liebe, H. J., 1989: MPM- An atmospheric millimeter wave propagation model. *Int. J. Infrared Millimeter Waves*, **10**, 631-650.

Liebe, H. J., P. W. Rosenkranz, and G. A. Hufford, 1992: Atmospheric 60 GHz oxygen spectrum: New laboratory measurements and line parameters. *J. Quant. Spectros. Radiat. Transfer*, **48**, 629-643.

Liu Q., F. Weng, and S. J. English, 2011: An improved fast microwave water emissivity model. *IEEE Trans. Geosci. Remote Sens.*, **49**, 1238-1250.

McCollum, J. R., and R. R. Ferraro, 2005: Microwave rainfall estimation over coasts. *J. Atmos. Oceanic Tech.*, **22**, 497-512.

Kummerow, C., 1993: On the accuracy of the Eddington Approximation for radiative transfer in the microwave frequencies. *J. Geophys. Res. – Atmos.*, **98**, 2757-2765.

Olson, W. S., P. Bauer, C. D. Kummerow, Y. Hong, and W.-K. Tao, 2001: A melting layer-model for passive/active microwave remote sensing applications. Part II: Simulation of TRMM observations. *J. Appl. Meteor.*, **40**, 1164-1179.

Olson, W. S., C. D. Kummerow, S. Yang, G. W. Petty, W.-K. Tao, T. L. Bell, S. A. Braun, Y. Wang, S. E. Lang, D. E. Johnson and C. Chiu. 2006: Precipitation and latent heating distributions from satellite passive microwave radiometry. Part I: Improved method and uncertainties. *J. Appl. Meteor. and Climatol.*, **45**, 702–720.

Prigent, C., F. Aires, and W. B. Rossow, 2006: Land surface microwave emissivities over the globe for a decade. *Bull. Amer. Met. Soc.*, **87**, 1573-1584.

Schwaller, M. R., and K. R. Morris, 2011: A ground validation network for the Global Precipitation Measurement Mission. *J. Atmos. Oceanic Tech.*, **28**, 301-319.

Testud, J., E. Le Bouar, E. Obligis, and M. Ali-Mehenni, 2000: The rain profiling algorithm applied to polarimetric weather radar. *J. Atmos. Oceanic Tech.*, **17**, 332-356.

Thurai, M., V. N. Bringi, L. D. Carey, P. Gatlin, E. Schultz, and W. A. Petersen, 2011: Estimating the accuracy of polarimetric radar-based retrievals of drop size distribution parameters and rain rate: An application of error variance separation using radar-derived spatial correlations. Submitted to the *Journal of Hydrometeorology*.

Tokay, A., and P. G. Bashor, 2010: An experimental study of small-scale variability of raindrop size distribution. *J. Appl. Meteor. and Climatol*., **49**, 2348-2365.

Vasiloff, S. V., D.-J. Seo, K. W. Howard, J. Zhang, D. H. Kitzmiller, M. G. Mullusky, W. F. Krajewski, E. A. Brandes, R. M. Rabin, D. S. Berkowitz, H. E. Brooks, J. A. McGinley, R. J. Kuligowski, and B. G. Brown, 2007: Improving QPE and very short term QPF. *Bull. Amer. Met. Soc*., **88**, 1899-1911.

Wolff, D. B., D. A. Marks, E. Amitai, D. S. Silberstein, B. L. Fisher, A. Tokay, J. Wang, and J. L. Pippitt, 2005: Ground validation for the Tropical Rainfall Measuring Mission (TRMM). *J. Atmos. Oceanic Tech.*, **22**, 365-380.

Appendix A. Listing of Input/Output Parameters

The listing of input and output parameters, below, is tentative. In particular, some of the input parameters will be provided by output of the Level 2 Radar Algorithm, and the submodules of that algorithm are currently being developed. Also, the output parameters of the GPM Combined Algorithm are still being reviewed. Still, the listing is fairly representative of parameters that will be input/output.

Input Parameters

This listing includes only those parameters that will be ingested from GPM Algorithms that are external to the Combined Radar-Radiometer Algorithm code. The given array size arguments correspond to:

nscan = number of DPR scans per granule, approximately 7900
nray = 49 rays of Normal Swath (NS) Ku band data
nrayMS = 25 rays of Matched Swath (MS) Ka band data
nrayHS = 24 rays of High sensitivity Swath (HS) Ka band data
nbin = 176 range bins of NS or MS radar data per ray
nbinHS = 88 range bins of HS Ka band data per ray
method = 6 methods for estimating path-integrated attenuation from the SRT
nNode = 5 bin nodes identified in the radar-defined DSD structure
nwind = 2 wind components: u, v
nwater = 2 water vapor and cloud liquid water profile parameters

nscan1 = number of lower-frequency (S1) GMI scans in the granule, approx. 2954
nscan2 = number of higher-frequency (S2) GMI scans in the granule, approx. 2954
npixel1 = 221 pixels per lower-frequency (S1) GMI scan
npixel2 = 221 pixels per higher-frequency (S2) GMI scan
nchannel1 = 9 channels of lower-frequency (S1) GMI data per pixel
nchannel2 = 4 channels of higher-frequency (S2) GMI data per pixel
nchUIA1 = 1 number of lower-frequency (S1) unique incidence angles
nchUIA2 = 1 number of higher-frequency (S2) unique incidence angles

<u>from the 2AKu Radar Algorithm</u>

Year
year of the Ku scan (2 byte integer, nscan); from the 2AKu Radar Algorithm.

Month
month of the Ku scan (1 byte integer, nscan); from the 2AKu Radar Algorithm.

DayOfMonth
day of month of the Ku scan (1 byte integer, nscan); from the 2AKu Radar Algorithm.

Hour
hour of the Ku scan (1 byte integer, nscan); from the 2AKu Radar Algorithm.

Minute
minute of the Ku scan (1 byte integer, nscan); from the 2AKu Radar Algorithm.

Second
second of the Ku scan (1 byte integer, nscan); from the 2AKu Radar Algorithm.

MilliSecond
millisecond of the Ku scan (2 byte integer, nscan); from the 2AKu Radar Algorithm.

DayOfYear
day of the year of the Ku scan (2 byte integer, nscan); from the 2AKu Radar Algorithm.

SecondOfDay
second of the day of the Ku scan (8 byte float, nscan); from the 2AKu Radar Algorithm.

Latitude
latitude of Ku footprint (4 byte float, nray x nscan); from the 2AKu Radar Algorithm.

Longitude
longitude of Ku footprint (4 byte float, nray x nscan); from the 2AKu Radar Algorithm.

elevation
altitude above the Earth ellipsoid of the surface gate in Ku ray (4 byte float, nray x nscan); from the 2AKu Radar Algorithm (PRE Submodule).

landSurfaceType
water/land/coast and surface type at Ku footprint location (4 byte integer, nray x nscan); from the 2AKu Radar Algorithm (PRE Submodule). Note that this information is used to interpret surface reference technique output.

localZenithAngle
local incidence angles of DPR ray relative to local zenith on the Earth ellipsoid (4 byte float, nray x nscan); from the 2AKu Radar Algorithm (PRE Submodule).

flagPrecip
flag indicating detection of precipation or no precipitation in Ku ray (4 byte integer, nray x nscan); from the 2AKu Radar Algorithm (PRE Submodule).

binRealSurface
surface range bin in Ku ray (2 byte integer, nray x nscan); from the 2AKu Radar Algorithm (PRE Submodule).

binStormTop
range bin of storm top in Ku ray (2 byte integer, nray x nscan); from the 2AKu Radar Algorithm (PRE Submodule).

heightStormTop
altitude of storm top in Ku ray (4 byte float, nray x nscan); from the 2AKu Radar Algorithm (PRE Submodule).

binClutterFreeBottom
range bin of the lowest clutter-free bin of Ku ray (2 byte integer, nray x nscan); from the 2AKu Radar Algorithm (PRE Submodule).

sigmaZeroMeasured
measured surface normalized radar backscattering cross-section at Ku (4 byte float, nray x nscan); from the 2AKu Radar Algorithm (PRE Submodule).

zFactorMeasured
measured reflectivity at Ku (2 byte integer, nbin x nray x nscan); from the 2AKu Radar Algorithm (PRE Submodule).

ellipsoidBinOffset
offset along Ku ray between earth ellipsoid and midpoint of surface range bin (4 byte float, nray x nscan); from the 2AKu Radar Algorithm (PRE Submodule).

binZeroDeg
range bin of the zero degree isotherm in Ku ray (2 byte integer, nray x nscan); from the 2AKu Radar Algorithm (VER Submodule).

heightZeroDeg
altitude of the zero degree isotherm in Ku ray (4 byte float, nray x nscan); from the 2AKu Radar Algorithm (VER Submodule).

flagBB
flag indicating the detection of a bright-band in Ku ray (4 byte integer, nray x nscan); from the 2AKu Radar Algorithm (CSF Submodule).

binBBPeak
range bin of the bright-band maximum reflectivity, if detected, in Ku ray (2 byte integer, nray x nscan); from the 2AKu Radar Algorithm (CSF Submodule).

heightBB
altitude of the bright-band maximum reflectivity, if detected, in Ku ray (4 byte float, nray x nscan); from the 2AKu Radar Algorithm (CSF Submodule).

qualityBB
quality flag for bright band detection in Ku ray (4 byte integer, nray x nscan); from the 2AKu Radar Algorithm (CSF Submodule).

type_Precip
classification of precipitation type in Ku ray (4 byte integer, nray x nscan); from the 2AKu Radar Algorithm (CSF Submodule).

qualityTypePrecip
quality of classification of precipitation type in Ku ray (4 byte integer, nray x nscan); from the 2AKu Radar Algorithm (CSF Submodule).

PIAalt
total 2-way path-integrated attenuation to the surface based upon surface reference technique methods for Ku (4 byte float, method x nray x nscan); from the 2AKu Radar Algorithm (SRT Submodule).

RFactorAlt
reliability factors of total 2-way path-integrated attenuation estimates based upon surface reference technique methods for Ku (4 byte float, method x nray x nscan); from the 2AKu Radar Algorithm (SRT Submodule).

PIAweight
weights of individual 2-way total path-integrated attenuation estimates to form effective estimate for Ku (4 byte float, method x nray x nscan); from the 2AKu Radar Algorithm (SRT Submodule).

pathAtten

effective total 2-way path-integrated attenuation to the surface based upon weighted averages of surface reference technique methods for Ku (4 byte float, nray x nscan); from the 2AKu Radar Algorithm (SRT Submodule).

reliabFactor
reliability factor of effective total 2-way path-integrated attenuation estimate based upon surface reference technique methods for Ku (4 byte float, nray x nscan); from the 2AKu Radar Algorithm (SRT Submodule).

reliabFlag
reliability flag for composite total 2-way path-integrated attenuation estimate based upon surface reference methods for Ku (2 byte integer, nray x nscan); from the 2AKu Radar Algorithm (SRT Submodule).

phase
particle phase based on Ku (1 byte integer, nbin x nray x nscan); from the 2AKu Radar Algorithm (DSD Submodule).

binNode
bin node for partitioning radar profile based on Ku (4 byte integer, nNode x nray x nscan); from the 2AKu Radar Algorithm (DSD Submodule).

flagParticle
particle flag based on Ku (1 byte integer, nbin x nray x nscan); from the 2AKu Radar Algorithm (DSD Submodule).

from the 2AKuENV Radar Algorithm

airTemperature
air temperature interpolated to Ku range bins (4 byte float, nbin x nray x nscan); from JMA data using the 2AKuENV Radar Algorithm (VER Submodule).

airPressure
air pressure interpolated to Ku range bins (4 byte float, nbin x nray x nscan); from JMA data using the 2AKuENV Radar Algorithm (VER Submodule).

waterVapor
water vapor density interpolated to Ku range bins (4 byte float, nwater x nray x nscan); from JMA data using the 2AKuENV Radar Algorithm (VER Submodule).

cloudLiquidWater
cloud liquid water content interpolated to Ku range bins (4 byte float, nwater x nray x nscan); from JMA data using the 2AKuENV Radar Algorithm (VER Submodule).

surfacePressure
surface air pressure interpolated to Ku footprint location (4 byte float, nray x nscan); from JMA data using the 2AKuENV Radar Algorithm (VER Submodule).

groundTemperature
surface skin temperature interpolated to Ku footprint location (4 byte float, nray x nscan); from JMA data using the 2AKuENV Radar Algorithm (VER Submodule).

surfaceWind
10-meter wind speed interpolated to Ku footprint location (4 byte float, nwind x nray x nscan); from JMA analysis using the 2AKuENV Radar Algorithm (VER Submodule).

from the 2ADPR Radar Algorithm (NS)

Year
year of the Ku scan (2 byte integer, nscan); from the 2ADPR Radar Algorithm (in NS).

Month
month of the Ku scan (1 byte integer, nscan); from the 2ADPR Radar Algorithm (in NS).

DayOfMonth
day of month of the Ku scan (1 byte integer, nscan); from the 2ADPR Radar Algorithm (in NS).

Hour
hour of the Ku scan (1 byte integer, nscan); from the 2ADPR Radar Algorithm (in NS).

Minute
minute of the Ku scan (1 byte integer, nscan); from the 2ADPR Radar Algorithm (in NS).

Second
second of the Ku scan (1 byte integer, nscan); from the 2ADPR Radar Algorithm (in NS).

MilliSecond
millisecond of the Ku scan (2 byte integer, nscan); from the 2ADPR Radar Algorithm (in NS).

DayOfYear
day of the year of the Ku scan (2 byte integer, nscan); from the 2ADPR Radar Algorithm (in NS).

SecondOfDay
second of the day of the Ku scan (8 byte float, nscan); from the 2ADPR Radar Algorithm (in NS).

Latitude
latitude of Ku footprint (4 byte float, nray x nscan); from the 2ADPR Radar Algorithm (in NS).

Longitude
longitude of Ku footprint (4 byte float, nray x nscan); from the 2ADPR Radar Algorithm (in NS).

elevation
altitude above the Earth ellipsoid of the surface gate in Ku ray (4 byte float, nray x nscan); from the 2ADPR Radar Algorithm (PRE Submodule in NS).

landSurfaceType
water/land/coast and surface type at Ku footprint location (4 byte integer, nray x nscan); from the 2ADPR Radar Algorithm (PRE Submodule in NS). Note that this information is used to interpret surface reference technique output.

localZenithAngle
local incidence angles of DPR ray relative to local zenith on the Earth ellipsoid (4 byte float, nray x nscan); from the 2ADPR Radar Algorithm (PRE Submodule in NS).

flagPrecip
flag indicating detection of precipation or no precipitation in Ku ray (4 byte integer, nray x nscan); from the 2ADPR Radar Algorithm (PRE Submodule in NS).

binRealSurface
surface range bin in Ku ray (2 byte integer, nray x nscan); from the 2ADPR Radar Algorithm (PRE Submodule in NS).

binStormTop
range bin of storm top in Ku ray (2 byte integer, nray x nscan); from the 2ADPR Radar Algorithm (PRE Submodule in NS).

heightStormTop
altitude of storm top in Ku ray (4 byte float, nray x nscan); from the 2ADPR Radar Algorithm (PRE Submodule in NS).

binClutterFreeBottom
range bin of the lowest clutter-free bin of Ku ray (2 byte integer, nray x nscan); from the 2ADPR Radar Algorithm (PRE Submodule in NS).

sigmaZeroMeasured
measured surface normalized radar backscattering cross-section at Ku (4 byte float, nray x nscan); from the 2ADPR Radar Algorithm (PRE Submodule in NS).

zFactorMeasured
measured reflectivity at Ku (2 byte integer, nbin x nray x nscan); from the 2ADPR Radar Algorithm (PRE Submodule in NS).

ellipsoidBinOffset
offset along Ku ray between earth ellipsoid and midpoint of surface range bin (4 byte float, nray x nscan); from the 2ADPR Radar Algorithm (PRE Submodule in NS).

binZeroDeg
range bin of the zero degree isotherm in Ku ray (2 byte integer, nray x nscan); from the 2ADPR Radar Algorithm (VER Submodule in NS).

heightZeroDeg
altitude of the zero degree isotherm in Ku ray (4 byte float, nray x nscan); from the 2ADPR Radar Algorithm (VER Submodule in NS).

flagBB
flag indicating the detection of a bright-band in Ku ray (4 byte integer, nray x nscan); from the 2ADPR Radar Algorithm (CSF Submodule in NS).

binBBPeak
range bin of the bright-band maximum reflectivity, if detected, in Ku ray (2 byte integer, nray x nscan); from the 2ADPR Radar Algorithm (CSF Submodule in NS).

heightBB
altitude of the bright-band maximum reflectivity, if detected, in Ku ray (4 byte float, nray x nscan); from the 2ADPR Radar Algorithm (CSF Submodule in NS).

qualityBB
quality flag for bright band detection in Ku ray (4 byte integer, nray x nscan); from the 2ADPR Radar Algorithm (CSF Submodule in NS).

type_Precip
classification of precipitation type in Ku ray (4 byte integer, nray x nscan); from the 2ADPR Radar Algorithm (CSF Submodule in NS).

qualityTypePrecip
quality of classification of precipitation type in Ku ray (4 byte integer, nray x nscan); from the 2ADPR Radar Algorithm (CSF Submodule in NS).

PIAalt
total 2-way path-integrated attenuation to the surface based upon surface reference technique methods for Ku (4 byte float, method x nray x nscan); from the 2ADPR Radar Algorithm (SRT Submodule in NS).

RFactorAlt
reliability factors of total 2-way path-integrated attenuation estimates based upon surface reference technique methods for Ku (4 byte float, method x nray x nscan); from the 2ADPR Radar Algorithm (SRT Submodule in NS).

PIAweight
weights of individual 2-way total path-integrated attenuation estimates to form effective estimate for Ku (4 byte float, method x nray x nscan); from the 2ADPR Radar Algorithm (SRT Submodule in NS).

pathAtten
effective total 2-way path-integrated attenuation to the surface based upon weighted averages of surface reference technique estimates for Ku (4 byte float, nray x nscan); from the 2ADPR Radar Algorithm (SRT Submodule in NS).

reliabFactor
reliability factor of effective total 2-way path-integrated attenuation estimate based upon surface reference technique methods for Ku (4 byte float, nray x nscan); from the 2ADPR Radar Algorithm (SRT Submodule in NS).

reliabFlag
reliability flag for effective total 2-way path-integrated attenuation estimate based upon surface reference methods for Ku (2 byte integer, nray x nscan); from the 2ADPR Radar Algorithm (SRT Submodule in NS).

phase
particle phase based on Ku (1 byte integer, nbin x nray x nscan); from the 2ADPR Radar Algorithm (DSD Submodule in NS).

binNode
bin node for partitioning radar profile based on Ku (4 byte integer, nNode x nray x nscan); from the 2ADPR Radar Algorithm (DSD Submodule in NS).

flagParticle
particle flag based on Ku (1 byte integer, nbin x nray x nscan); from the 2ADPR Radar Algorithm (DSD Submodule in NS).

from the 2ADPR Radar Algorithm (MS)

Year
year of the Ka scan (2 byte integer, nscan); from the 2ADPR Radar Algorithm (in MS).

Month
month of the Ka scan (1 byte integer, nscan); from the 2ADPR Radar Algorithm (in MS).

DayOfMonth
day of month of the Ka scan (1 byte integer, nscan); from the 2ADPR Radar Algorithm (in MS).

Hour
hour of the Ka scan (1 byte integer, nscan); from the 2ADPR Radar Algorithm (in MS).

Minute
minute of the Ka scan (1 byte integer, nscan); from the 2ADPR Radar Algorithm (in MS).

Second
second of the Ka scan (1 byte integer, nscan); from the 2ADPR Radar Algorithm (in MS).

MilliSecond
millisecond of the Ka scan (2 byte integer, nscan); from the 2ADPR Radar Algorithm (in MS).

DayOfYear
day of the year of the Ka scan (2 byte integer, nscan); from the 2ADPR Radar Algorithm (in MS).

SecondOfDay
second of the day of the Ka scan (8 byte float, nscan); from the 2ADPR Radar Algorithm (in MS).

Latitude
latitude of Ka footprint (4 byte float, nrayMS x nscan); from the 2ADPR Radar Algorithm (in MS).

Longitude
longitude of Ka footprint (4 byte float, nrayMS x nscan); from the 2ADPR Radar Algorithm (in MS).

elevation
altitude above the Earth ellipsoid of the surface gate in Ka ray (4 byte float, nrayMS x nscan); from the 2ADPR Radar Algorithm (PRE Submodule in MS).

landSurfaceType
water/land/coast and surface type at Ka footprint location (4 byte integer, nrayMS x nscan); from the 2ADPR Radar Algorithm (PRE Submodule in MS). Note that this information is used to interpret surface reference technique output.

localZenithAngle
local incidence angles of DPR ray relative to local zenith on the Earth ellipsoid (4 byte float, nrayMS x nscan); from the 2ADPR Radar Algorithm (PRE Submodule in MS).

flagPrecip
flag indicating detection of precipation or no precipitation in Ka ray (4 byte integer, nrayMS x nscan); from the 2ADPR Radar Algorithm (PRE Submodule in MS).

binRealSurface
surface range bin in Ka ray (2 byte integer, nrayMS x nscan); from the 2ADPR Radar Algorithm (PRE Submodule in MS).

binStormTop
range bin of storm top in Ka ray (2 byte integer, nrayMS x nscan); from the 2ADPR Radar Algorithm (PRE Submodule in MS).

heightStormTop

altitude of storm top in Ka ray (4 byte float, nrayMS x nscan); from the 2ADPR Radar Algorithm (PRE Submodule in MS).

binClutterFreeBottom
range bin of the lowest clutter-free bin of Ka ray (2 byte integer, nrayMS x nscan); from the 2ADPR Radar Algorithm (PRE Submodule in MS).

sigmaZeroMeasured
measured surface normalized radar backscattering cross-section at Ka (4 byte float, nrayMS x nscan); from the 2ADPR Radar Algorithm (PRE Submodule in MS).

zFactorMeasured
measured reflectivity at Ka (2 byte integer, nbin x nrayMS x nscan); from the 2ADPR Radar Algorithm (PRE Submodule in MS).

ellipsoidBinOffset
offset along Ka ray between earth ellipsoid and midpoint of surface range bin (4 byte float, nrayMS x nscan); from the 2ADPR Radar Algorithm (PRE Submodule in MS).

binZeroDeg
range bin of the zero degree isotherm in Ka ray (2 byte integer, nrayMS x nscan); from the 2ADPR Radar Algorithm (VER Submodule in MS).

heightZeroDeg
altitude of the zero degree isotherm in Ka ray (4 byte float, nrayMS x nscan); from the 2ADPR Radar Algorithm (VER Submodule in MS).

flagBB
flag indicating the detection of a bright-band in Ka ray (4 byte integer, nrayMS x nscan); from the 2ADPR Radar Algorithm (CSF Submodule in MS).

binBBPeak
range bin of the bright-band maximum reflectivity, if detected, in Ka ray (2 byte integer, nrayMS x nscan); from the 2ADPR Radar Algorithm (CSF Submodule in MS).

heightBB
altitude of the bright-band maximum reflectivity, if detected, in Ka ray (4 byte float, nrayMS x nscan); from the 2ADPR Radar Algorithm (CSF Submodule in MS).

qualityBB
quality flag for bright band detection in Ka ray (4 byte integer, nrayMS x nscan); from the 2ADPR Radar Algorithm (CSF Submodule in MS).

type_Precip
classification of precipitation type in Ka ray (4 byte integer, nrayMS x nscan); from the 2ADPR Radar Algorithm (CSF Submodule in MS).

qualityTypePrecip
quality of classification of precipitation type in Ka ray (4 byte integer, nrayMS x nscan); from the 2ADPR Radar Algorithm (CSF Submodule in MS).

PIAalt
total 2-way path-integrated attenuation to the surface based upon surface reference technique methods for Ka (4 byte float, method x nrayMS x nscan); from the 2ADPR Radar Algorithm (SRT Submodule in MS).

RFactorAlt
reliability factors of total 2-way path-integrated attenuation estimates based upon surface reference technique methods for Ka (4 byte float, method x nrayMS x nscan); from the 2ADPR Radar Algorithm (SRT Submodule in MS).

PIAweight
weights of individual 2-way total path-integrated attenuation estimates to form effective estimates for Ka (4 byte float, method x nrayMS x nscan); from the 2ADPR Radar Algorithm (SRT Submodule in MS).

pathAtten
effective total 2-way path-integrated attenuation to the surface based upon weighted averages of surface reference technique estimates for Ka (4 byte float, nrayMS x nscan); from the 2ADPR Radar Algorithm (SRT Submodule in MS).

reliabFactor
reliability factor of effective total 2-way path-integrated attenuation estimate based upon surface reference technique methods for Ka (4 byte float, nrayMS x nscan); from the 2ADPR Radar Algorithm (SRT Submodule in MS).

reliabFlag
reliability flag for composite total 2-way path-integrated attenuation estimate based upon surface reference methods for Ka (2 byte integer, nrayMS x nscan); from the 2ADPR Radar Algorithm (SRT Submodule in MS).

phase
particle phase based on Ka (1 byte integer, nbin x nrayMS x nscan); from the 2ADPR Radar Algorithm (DSD Submodule in MS).

binNode
bin node for partitioning radar profile based on Ka (4 byte integer, nNode x nrayMS x nscan); from the 2ADPR Radar Algorithm (DSD Submodule in MS).

flagParticle
particle flag based on Ka (1 byte integer, nbin x nrayMS x nscan); from the 2ADPR Radar Algorithm (DSD Submodule in MS).

from the 2ADPR Radar Algorithm (HS)

Year
year of the Ka scan (2 byte integer, nscan); from the 2ADPR Radar Algorithm (in HS).

Month
month of the Ka scan (1 byte integer, nscan); from the 2ADPR Radar Algorithm (in HS).

DayOfMonth
day of month of the Ka scan (1 byte integer, nscan); from the 2ADPR Radar Algorithm (in HS).

Hour
hour of the Ka scan (1 byte integer, nscan); from the 2ADPR Radar Algorithm (in HS).

Minute
minute of the Ka scan (1 byte integer, nscan); from the 2ADPR Radar Algorithm (in HS).

Second
second of the Ka scan (1 byte integer, nscan); from the 2ADPR Radar Algorithm (in HS).

MilliSecond
millisecond of the Ka scan (2 byte integer, nscan); from the 2ADPR Radar Algorithm (in HS).

DayOfYear
day of year of the Ka scan (2 byte integer, nscan); from the 2ADPR Radar Algorithm (in HS).

SecondOfDay
second of day of the Ka scan (8 byte float, nscan); from the 2ADPR Radar Algorithm (in HS).

Latitude
latitude of Ka footprint (4 byte float, nrayHS x nscan); from the 2ADPR Radar Algorithm (in HS).

Longitude
longitude of Ka footprint (4 byte float, nrayHS x nscan); from the 2ADPR Radar Algorithm (in HS).

elevation
altitude above the Earth ellipsoid of the surface gate in Ka ray (4 byte float, nrayHS x nscan); from the 2ADPR Radar Algorithm (PRE Submodule in HS).

landSurfaceType
water/land/coast and surface type at Ka footprint location (4 byte integer, nrayHS x nscan); from the 2ADPR Radar Algorithm (PRE Submodule in HS). Note that this information is used to interpret surface reference technique output.

localZenithAngle
local incidence angles of DPR ray relative to local zenith on the Earth ellipsoid (4 byte float, nrayHS x nscan); from the 2ADPR Radar Algorithm (PRE Submodule in HS).

flagPrecip
flag indicating detection of precipation or no precipitation in Ka ray (4 byte integer, nrayHS x nscan); from the 2ADPR Radar Algorithm (PRE Submodule in HS).

binRealSurface
surface range bin in Ka ray (2 byte integer, nrayHS x nscan); from the 2ADPR Radar Algorithm (PRE Submodule in HS).

binStormTop
range bin of storm top in Ka ray (2 byte integer, nrayHS x nscan); from the 2ADPR Radar Algorithm (PRE Submodule in HS).

heightStormTop
altitude of storm top in Ka ray (4 byte float, nrayHS x nscan); from the 2ADPR Radar Algorithm (PRE Submodule in HS).

binClutterFreeBottom
range bin of the lowest clutter-free bin of Ka ray (2 byte integer, nrayHS x nscan); from the 2ADPR Radar Algorithm (PRE Submodule in HS).

sigmaZeroMeasured
measured surface normalized radar backscattering cross-section at Ka (4 byte float, nrayHS x nscan); from the 2ADPR Radar Algorithm (PRE Submodule in HS).

zFactorMeasured

measured reflectivity at Ka (2 byte integer, nbinHS x nrayHS x nscan); from the 2ADPR Radar Algorithm (PRE Submodule in HS).

ellipsoidBinOffset
offset along Ka ray between earth ellipsoid and midpoint of surface range bin (4 byte float, nrayHS x nscan); from the 2ADPR Radar Algorithm (PRE Submodule in HS).

binZeroDeg
range bin of the zero degree isotherm in Ka ray (2 byte integer, nrayHS x nscan); from the 2ADPR Radar Algorithm (VER Submodule in HS).

heightZeroDeg
altitude of the zero degree isotherm in Ka ray (4 byte float, nrayHS x nscan); from the 2ADPR Radar Algorithm (VER Submodule in HS).

flagBB
flag indicating the detection of a bright-band in Ka ray (4 byte integer, nrayHS x nscan); from the 2ADPR Radar Algorithm (CSF Submodule in HS).

binBBPeak
range bin of the bright-band maximum reflectivity, if detected, in Ka ray (2 byte integer, nrayHS x nscan); from the 2ADPR Radar Algorithm (CSF Submodule in HS).

heightBB
altitude of the bright-band maximum reflectivity, if detected, in Ka ray (4 byte float, nrayHS x nscan); from the 2ADPR Radar Algorithm (CSF Submodule in HS).

qualityBB
quality flag for bright band detection in Ka ray (4 byte integer, nrayHS x nscan); from the 2ADPR Radar Algorithm (CSF Submodule in HS).

type_Precip
classification of precipitation type in Ka ray (4 byte integer, nrayHS x nscan); from the 2ADPR Radar Algorithm (CSF Submodule in HS).

qualityTypePrecip
quality of classification of precipitation type in Ka ray (4 byte integer, nrayHS x nscan); from the 2ADPR Radar Algorithm (CSF Submodule in HS).

PIAalt
total 2-way path-integrated attenuation to the surface based upon surface reference technique methods for Ka (4 byte float, method x nrayHS x nscan); from the 2ADPR Radar Algorithm (SRT Submodule in HS).

RFactorAlt
reliability factors of total 2-way path-integrated attenuation estimates based upon surface reference technique methods for Ka (4 byte float, method x nrayHS x nscan); from the 2ADPR Radar Algorithm (SRT Submodule in HS).

PIAweight
weights of individual 2-way total path-integrated attenuation estimates to form effective estimate for Ka (4 byte float, method x nrayHS x nscan); from the 2ADPR Radar Algorithm (SRT Submodule in HS).

pathAtten

effective total 2-way path-integrated attenuation to the surface based upon weighted averages of surface reference technique estimates for Ka (4 byte float, nrayHS x nscan); from the 2ADPR Radar Algorithm (SRT Submodule in HS).

reliabFactor
reliability factor of effective total 2-way path-integrated attenuation estimate based upon surface reference technique methods for Ka (4 byte float, nrayHS x nscan); from the 2ADPR Radar Algorithm (SRT Submodule in HS).

reliabFlag
reliability flag for effective total 2-way path-integrated attenuation estimate based upon surface reference methods for Ka (2 byte integer, nrayHS x nscan); from the 2ADPR Radar Algorithm (SRT Submodule in HS).

phase
particle phase based on Ka (1 byte integer, nbinHS x nrayHS x nscan); from the 2ADPR Radar Algorithm (DSD Submodule in HS).

binNode
bin node for partitioning radar profile based on Ka (4 byte integer, nNode x nrayHS x nscan); from the 2ADPR Radar Algorithm (DSD Submodule in HS).

flagParticle
particle flag based on Ka (1 byte integer, nbinHS x nrayHS x nscan); from the 2ADPR Radar Algorithm (DSD Submodule in HS).

from the 2ADPRENV Radar Algorithm (HS)

airTemperature
air temperature interpolated to Ka range bins (4 byte float, nbinHS x nrayHS x nscan); from JMA data using the 2ADPRENV Radar Algorithm (VER Submodule in HS).

airPressure
air pressure interpolated to Ka range bins (4 byte float, nbinHS x nrayHS x nscan); from JMA data using the 2ADPRENV Radar Algorithm (VER Submodule in HS).

waterVapor
water vapor density interpolated to Ka range bins (4 byte float, nwater x nrayHS x nscan); from JMA data using the 2ADPRENV Radar Algorithm (VER Submodule in HS).

cloudLiquidWater
cloud liquid water content interpolated to Ka range bins (4 byte float, nwater x nrayHS x nscan); from JMA data using the 2ADPRENV Radar Algorithm (VER Submodule in HS).

surfacePressure
surface air pressure interpolated to Ka footprint location (4 byte float, nrayHS x nscan); from JMA data using the 2ADPRENV Radar Algorithm (VER Submodule in HS).

groundTemperature
surface skin temperature interpolated to Ka footprint location (4 byte float, nrayHS x nscan); from JMA data using the 2ADPRENV Radar Algorithm (VER Submodule in HS).

surfaceWind
10-meter wind speed interpolated to Ka footprint location (4 byte float, nwind x nrayHS x nscan); from JMA analysis using the 2ADPRENV Radar Algorithm (VER Submodule in HS).

from the 1CGMI Algorithm (S1)

Year
year of the GMI scan (2 byte integer, nscan1) from the 1CGMI Algorithm (in S1).

Month
month of the GMI scan (1 byte integer, nscan1) from the 1CGMI Algorithm (in S1).

DayOfMonth
day of month of the GMI scan (1 byte integer, nscan1) from the 1CGMI Algorithm (in S1).

Hour
hour of the GMI scan (1 byte integer, nscan1) from the 1CGMI Algorithm (in S1).

Minute
minute of the GMI scan (1 byte integer, nscan1) from the 1CGMI Algorithm (in S1).

Second
second of the GMI scan (1 byte integer, nscan1) from the 1CGMI Algorithm (in S1).

MilliSecond
millisecond of the GMI scan (2 byte integer, nscan1) from the 1CGMI Algorithm (in S1).

DayOfYear
day of year of the GMI scan (2 byte integer, nscan1); from the 1CGMI Algorithm (in S1).

SecondOfDay
second of day of the GMI scan (8 byte float, nscan1); from the 1CGMI Algorithm (in S1).

Latitude
latitude of the GMI footprint (4 byte float, npixel1 x nscan1); from the 1CGMI Algorithm (in S1).

Longitude
longitude of the GMI footprint (4 byte float, npixel1 x nscan1); from the 1CGMI Algorithm (in S1).

Quality
quality of the lower-frequency calibrated brightness temperatures (1 byte integer, npixel1 x nscan1); from the 1CGMI Algorithm (in S1).

incidenceAngle
earth incidence angle of the GMI lower-frequency data (4 byte float, nchUIA1 x npixel1 x nscan1); from the 1CGMI Algorithm (in S1).

sunGlintAngle
sun glint angles of the GMI lower-frequency data (1 byte integer, nchUIA1 x npixel1 x nscan1); from the 1CGMI Algorithm (in S1).

incidenceAngleIndex
index of the incidence angle array for each lower-frequency channel (1 byte integer, nchannel1 x nscan1); from the 1CGMI Algorithm (in S1).

Tc
common calibrated GMI brightness temperatures in the lower-frequency data swath (4 byte float, nchannel1 x npixel1 x nscan1); from the 1CGMI Algorithm (in S1).

from the 1CGMI Algorithm (S2)

Year
year of the GMI scan (2 byte integer, nscan2) from the 1CGMI Algorithm (in S2).

Month
month of the GMI scan (1 byte integer, nscan2) from the 1CGMI Algorithm (in S2).

DayOfMonth
day of month of the GMI scan (1 byte integer, nscan2) from the 1CGMI Algorithm (in S2).

Hour
hour of the GMI scan (1 byte integer, nscan2) from the 1CGMI Algorithm (in S2).

Minute
minute of the GMI scan (1 byte integer, nscan2) from the 1CGMI Algorithm (in S2).

Second
second of the GMI scan (1 byte integer, nscan2) from the 1CGMI Algorithm (in S2).

MilliSecond
millisecond of the GMI scan (2 byte integer, nscan2) from the 1CGMI Algorithm (in S2).

DayOfYear
day of year of the GMI scan (2 byte integer, nscan2); from the 1CGMI Algorithm (in S2).

SecondOfDay
second of day of the GMI scan (8 byte float, nscan2); from the 1CGMI Algorithm (in S2).

Latitude
latitude of the GMI footprint (4 byte float, npixel2 x nscan2); from the 1CGMI Algorithm (in S2).

Longitude
longitude of the GMI footprint (4 byte float, npixel2 x nscan2); from the 1CGMI Algorithm (in S2).

Quality
quality of the higher-frequency calibrated brightness temperatures (1 byte integer, npixel2 x nscan2); from the 1CGMI Algorithm (in S2).

incidenceAngle
earth incidence angles of the GMI higher-frequency data (4 byte float, nchUIA2 x npixel2 x nscan2); from the 1CGMI Algorithm (in S2).

sunGlintAngle
sun glint angles of the GMI higher-frequency data (1 byte integer, nchUIA2 x npixel2 x nscan2); from the 1CGMI Algorithm (in S2).

incidenceAngleIndex
index of the incidence angle array for each higher-frequency channel (1 byte integer, nchannel2 x nscan2); from the 1CGMI Algorithm (in S2).

Tc
common calibrated GMI brightness temperatures in the higher-frequency data swath (4 byte float, nchannel2 x npixel2 x nscan2); from the 1CGMI Algorithm (in S2).

Output Parameters (Standard Processing)

Note standard output products are sampled at 250 m vertical resolution. The given array size arguments correspond to:

nscan = number of DPR scans per granule, approximately 7900
nrayS1 = 49 rays in each Ku band (S1) scan
nrayS2 = 25 rays in each matched Ku-Ka (S2) scan
nbinC = 88 vertical range bins at 250 m intervals
nPSD = 3 parameters for describing the precipitation particle size distribution
nAB = 2 power law parameters to describe particle densities
nKuKa = 2 indices for the Ku and Ka channels
nchan = 15 GMI channels, including separate accounting for the double side-band channels.

<u>from the 2BCMB Combined Radar-Radiometer Algorithm (S1)</u>

Year
year of the Ku band scan (2 byte integer, nscan); from the 2BCMB Combined Algorithm (in S1).

Month
month of the Ku band scan (1 byte integer, nscan); from the 2BCMB Combined Algorithm (in S1).

DayOfMonth
day of month of the Ku band scan (1 byte integer, nscan); from the 2BCMB Combined Algorithm (in S1).

Hour
hour of the Ku band scan (1 byte integer, nscan); from the 2BCMB Combined Algorithm (in S1).

Minute
minute of the Ku band scan (1 byte integer, nscan); from the 2BCMB Combined Algorithm (in S1).

Second
second of the Ku band scan (1 byte integer, nscan); from the 2BCMB Combined Algorithm (in S1).

MilliSecond
millisecond of the Ku band scan (2 byte integer, nscan); from the 2BCMB Combined Algorithm (in S1).

DayOfYear
day of year of the Ku band scan (2 byte integer, nscan); from the 2BCMB Combined Algorithm (in S1).

SecondOfDay
second of day of the Ku band scan (8 byte float, nscan); from the 2BCMB Combined Algorithm (in S1).

Latitude
latitude of Ku band footprint (4 byte float, nrayS1 x nscan); from the 2BCMB Combined Algorithm (in S1).

Longitude
longitude of Ku band footprint (4 byte float, nrayS1 x nscan); from the 2BCMB Combined Algorithm (in S1).

surfaceElevation
altitude above the Earth ellipsoid of the surface gate in Ku band ray (4 byte float, nrayS1 x nscan); from the 2BCMB Combined Algorithm (in S1).

surfaceType
water/land/coast and surface type at Ku band footprint location (4 byte integer, nrayS1 x nscan); from the 2BCMB Combined Algorithm (in S1).

localZenithAngle
local incidence angle of Ku band ray relative to local zenith on the Earth ellipsoid (4 byte float, nrayS1 x nscan); from the 2BCMB Combined Algorithm (in S1).

precipitationFlag
flag indicating detection of precipation or no precipitation in Ku band ray (4 byte integer, nrayS1 x nscan); from the 2BCMB Combined Algorithm (in S1).

surfaceRangeBin
surface range bin in Ku band ray (2 byte integer, nrayS1 x nscan); from the 2BCMB Combined Algorithm (in S1).

lowestClutterFreeBin
lowest clutter free bin in Ku band ray (2 byte integer, nrayS1 x nscan); from the 2BCMB Combined Algorithm (in S1).

ellipsoidBinOffset
offset along Ku ray between earth ellipsoid and midpoint of surface range bin (4 byte float, nrayS1 x nscan); from the 2BCMB Combined Algorithm (in S1).

stormTopBin
storm top range bin in Ku band ray (2 byte integer, nrayS1 x nscan); from the 2BCMB Combined Algorithm (in S1).

stormTopAltitude
storm top altitude in Ku band ray (4 byte float, nrayS1 x nscan); from the 2BCMB Combined Algorithm (in S1).

precipitationType
classification of precipitation type in Ku band ray (4 byte integer, nrayS1 x nscan); from the 2BCMB Combined Algorithm (in S1).

precipTypeQualityFlag
quality of classification of precipitation type in Ku band ray (4 byte integer, nrayS1 x nscan); from the 2BCMB Combined Algorithm (in S1).

piaEffective
effective total 2-way path-integrated attenuation to the surface at Ku band, based upon weighted averages of surface reference technique estimates (4 byte float, nrayS1 x nscan); from the 2BCMB Combined Algorithm (in S1).

piaEffectiveSigma
uncertainty of effective total 2-way path-integrated attenuation at Ku band based upon surface reference technique methods (4 byte float, nrayS1 x nscan); from the 2BCMB Combined Algorithm (in S1).

piaEffectiveReliabFlag
reliability flag of the effective total 2-way path-integrated attenuation at Ku band, based upon weighted averages of surface reference technique estimates (2 byte integer, nrayS1 x nscan); from the 2BCMB Combined Algorithm (in S1).

surfaceAirPressureOut
surface air pressure at the Ku band footprint location (4 byte float, nrayS1 x nscan); from the 2BCMB Combined Algorithm (in S1).

groundTemperatureOut
surface skin temperature at the Ku band footprint location (4 byte float, nrayS1 x nscan); from the 2BCMB Combined Algorithm (in S1).

airPressureOut
air pressure along the Ku band ray at 250 m sampling resolution (2 byte integer, nbinC x nrayS1 x nscan); from the 2BCMB Combined Algorithm (in S1).

airTemperatureOut
air temperature along the Ku band rays at 250 m sampling resolution (2 byte integer, nbinC x nrayS1 x nscan); from the 2BCMB Combined Algorithm (in S1).

vaporDensityOut
vapor density along the Ku band ray at 250 m sampling resolution (2 byte integer, nbinC x nrayS1 x nscan); from the 2BCMB Combined Algorithm (in S1).

cloudLiqWaterContOut
cloud liquid water content along the Ku band ray at 250 m sampling resolution (2 byte integer, nbinC x nrayS1 x nscan); from the 2BCMB Combined Algorithm (in S1).

cloudIceWaterContOut
cloud ice liquid-equivalent water content along the Ku band ray at 250 m sampling resolution (2 byte integer, nbinC x nrayS1 x nscan); from the 2BCMB Combined Algorithm (in S1).

rainPSDparamOut
liquid precipitation drop-size distribution parameters ($\log(N_w)$, D_o, μ) along the Ku band ray at 250 m sampling resolution (2 byte integer, nPSD x nbinC x nrayS1 x nscan); from the 2BCMB Combined Algorithm (in S1).

rainPSDparamSigmaOut
liquid precipitation drop-size distribution parameter ($\log(N_w)$, D_o, μ) uncertainties along the Ku band ray at 250 m sampling resolution (2 byte integer, nPSD x nbinC x nrayS1 x nscan); from the 2BCMB Combined Algorithm (in S1).

icePSDparamOut
ice-phase precipitation liquid-equivalent drop-size distribution parameters ($\log(N_w)$, D_o, μ) along the Ku band ray at 250 m sampling resolution (2 byte integer. nPSD x nbinC x nrayS1 x nscan); from the 2BCMB Combined Algorithm (in S1).

icePSDparamSigmaOut

ice-phase precipitation liquid-equivalent drop-size distribution parameter ($\log(N_w)$, D_o, μ) uncertainties along the Ku band ray at 250 m vertical resolution (2 byte integer, nPSD x nbinC x nrayS1 x nscan); from the 2BCMB Combined Algorithm (in S1).

iceDensityOut
density of ice-phase precipitation expressed as a power law (α, β, of $\rho_{ice} = \alpha D^{\beta}$, where D is particle melted diameter) along the Ku ray at 250 m sampling resolution (2 byte integer, nAB x nbinC x nrayS1 x nscan); from the 2BCMB Combined Algorithm (in S1).

iceMeltFractionOut
fraction of melting ice particle liquid-equivalent water content in the form of liquid water along the Ku band ray at 250 m sampling resolution (2 byte integer, nbinC x nrayS1 x nscan); from the 2BCMB Combined Algorithm (in S1).

surfRainRateOut
surface liquid precipitation rate at Ku footprint location (4 byte float, nrayS1 x nscan); from the 2BCMB Combined Algorithm (in S1).

surfRainRateSigmaOut
surface liquid precipitation rate uncertainty at Ku footprint location (4 byte float, nrayS1 x nscan); from the 2BCMB Combined Algorithm (in S1).

surfPrecipIceRateOut
surface ice-phase precipitation rate at Ku footprint location (4 byte float, nrayS1 x nscan); from the 2BCMB Combined Algorithm (in S1).

surfPrecipIceRateSigmaOut
surface ice-phase precipitation rate uncertainty at Ku footprint location (4 byte float, nrayS1 x nscan); from the 2BCMB Combined Algorithm (in S1).

tenMeterWindSpeedOut
10-meter wind speed at Ku footprint location (4 byte float, nrayS1 x nscan); from the 2BCMB Combined Algorithm (in S1).

surfaceEmissivityOut
microwave surface emissivities at the GMI channel frequencies/polarizations and viewing angle, including separate emissivities for the double side-band channels at 183.3 ± 7 and 183.3 ± 3 GHz, at Ku footprint location (4 byte float, nchan x nrayS1 x nscan); from the 2BCMB Combined Algorithm (in S1).

simulatedBrightTempOut
upwelling microwave surface brightness temperatures at the GMI channel frequencies/polarizations and viewing angle, but at Ku band footprint resolution, including separate brightness temperatures for the double side-band channels at 183.3 ± 7 and 183.3 ± 3 GHz (4 byte float, nchan x nrayS1 x nscan); from the 2BCMB Combined Algorithm (in S1).

piaOut
total path-integrated attenuation at Ku (4 byte float, nrayS1 x nscan); from the 2BCMB Combined Algorithm (in S1).

correctedReflectFactorOut
attenuation-corrected radar reflectivity factor along Ku ray at 250 m sampling resolution (2 byte integer, nbinC x nrayS1 x nscan); from the Combined Algorithm.

<u>from the 2BCMB Combined Radar-Radiometer Algorithm (S2)</u>

Year

year of the Ku/Ka scan (2 byte integer, nscan); from the 2BCMB Combined Algorithm (in S2).

Month
month of the Ku/Ka scan (1 byte integer, nscan); from the 2BCMB Combined Algorithm (in S2).

DayOfMonth
day of month of the Ku/Ka scan (1 byte integer, nscan); from the 2BCMB Combined Algorithm (in S2).

Hour
hour of the Ku/Ka scan (1 byte integer, nscan); from the 2BCMB Combined Algorithm (in S2).

Minute
minute of the Ku/Ka scan (1 byte integer, nscan); from the 2BCMB Combined Algorithm (in S2).

Second
second of the Ku/Ka scan (1 byte integer, nscan); from the 2BCMB Combined Algorithm (in S2).

MilliSecond
millisecond of the Ku/Ka scan (2 byte integer, nscan); from the 2BCMB Combined Algorithm (in S2).

DayOfYear
day of year of the Ku/Ka scan (2 byte integer, nscan); from the 2BCMB Combined Algorithm (in S2).

SecondOfDay
second of day of the Ku/Ka scan (8 byte float, nscan); from the 2BCMB Combined Algorithm (in S2).

Latitude
latitude of Ku/Ka footprint (4 byte float, nrayS2 x nscan); from the 2BCMB Combined Algorithm (in S2).

Longitude
longitude of Ku/Ka footprint (4 byte float, nrayS2 x nscan); from the 2BCMB Combined Algorithm (in S2).

surfaceElevation
altitude above the Earth ellipsoid of the surface gate in Ku/Ka ray (4 byte float, nKuKa x nrayS2 x nscan); from the 2BCMB Combined Algorithm (in S2).

surfaceType
water/land/coast and surface type at Ku/Ka footprint location (4 byte integer, nrayS2 x nscan); from the 2BCMB Combined Algorithm (in S2).

localZenithAngle
local incidence angle of Ku/Ka ray relative to local zenith on the Earth ellipsoid (4 byte float, nrayS2 x nscan); from the 2BCMB Combined Algorithm (in S2).

precipitationFlag

flag indicating detection of precipation or no precipitation in Ku/Ka ray (4 byte integer, nrayS2 x nscan); from the 2BCMB Combined Algorithm (in S2).

surfaceRangeBin
surface range bin in Ku/Ka ray (2 byte integer, nKuKa x nrayS2 x nscan); from the 2BCMB Combined Algorithm (in S2).

lowestClutterFreeBin
lowest clutter free bin in Ku/Ka ray (2 byte integer, nKuKa x nrayS2 x nscan); from the 2BCMB Combined Algorithm (in S2).

ellipsoidBinOffset
offset along the Ku/Ka ray between earth ellipsoid and midpoint of surface range bin (4 byte float, nKuKa x nrayS2 x nscan); from the 2BCMB Combined Algorithm (in S2).

stormTopBin
storm top range bin in Ku/Ka ray (2 byte integer, nKuKa x nrayS2 x nscan); from the 2BCMB Combined Algorithm (in S2).

stormTopAltitude
storm top altitude in Ku/Ka ray (4 byte float, nKuKa x nrayS2 x nscan); from the 2BCMB Combined Algorithm (in S2).

precipitationType
classification of precipitation type in Ku/Ka ray (4 byte integer, nrayS2 x nscan); from the 2BCMB Combined Algorithm (in S2).

precipTypeQualityFlag
quality of classification of precipitation type in Ku/Ka ray (4 byte integer, nrayS2 x nscan); from the 2BCMB Combined Algorithm (in S2).

piaEffective
effective total 2-way path-integrated attenuation to the surface at Ku and Ka band, based upon weighted averages of surface reference technique methods (4 byte float, nKuKa x nrayS2 x nscan); from the 2BCMB Combined Algorithm (in S2).

piaEffectiveSigma
uncertainty of effective total 2-way path-integrated attenuation at Ku and Ka band based upon surface reference technique estimates (4 byte float, nKuKa x nrayS2 x nscan); from the 2BCMB Combined Algorithm (in S2).

piaEffectiveReliabFlag
reliability flag of the effective total 2-way path-integrated attenuation at Ku and Ka band, based upon weighted averages of surface reference technique estimates (2 byte integer, nKuKa x nrayS2 x nscan); from the 2BCMB Combined Algorithm (in S2).

surfaceAirPressureOut
surface air pressure at the Ku/Ka footprint locations (4 byte float, nrayS2 x nscan); from the 2BCMB Combined Algorithm (in S2).

groundTemperatureOut
surface skin temperature at the Ku/Ka footprint locations (4 byte float, nrayS2 x nscan); from the 2BCMB Combined Algorithm (in S2).

airPressureOut

air pressure along the Ku/Ka ray at 250 m sampling resolution (2 byte integer, nbinC x nrayS2 x nscan); from the 2BCMB Combined Algorithm (in S2).

airTemperatureOut
air temperature along the Ku/Ka ray at 250 m sampling resolution (2 byte integer, nbinC x nrayS2 x nscan); from the 2BCMB Combined Algorithm (in S2).

vaporDensityOut
vapor density along the Ku/Ka ray at 250 m sampling resolution (2 byte integer, nbinC x nrayS2 x nscan); from the 2BCMB Combined Algorithm (in S2).

cloudLiqWaterContOut
cloud liquid water content along the Ku/Ka ray at 250 m sampling resolution (2 byte integer, nbinC x nrayS2 x nscan); from the 2BCMB Combined Algorithm (in S2).

cloudIceWaterContOut
cloud ice liquid-equivalent water content along the Ku/Ka ray at 250 m sampling resolution (2 byte integer, nbinC x nrayS2 x nscan); from the 2BCMB Combined Algorithm (in S2).

rainPSDparamOut
liquid precipitation drop-size distribution parameters ($\log(N_w)$, D_o, μ) along the Ku/Ka ray at 250 m sampling resolution (2 byte integer, nPSD x nbinC x nrayS2 x nscan); from the 2BCMB Combined Algorithm (in S2).

rainPSDparamSigmaOut
liquid precipitation drop-size distribution parameter ($\log(N_w)$, D_o, μ) uncertainties along the Ku/Ka ray at 250 m sampling resolution (2 byte integer, nPSD x nbinC x nrayS2 x nscan); from the 2BCMB Combined Algorithm (in S2).

icePSDparamOut
ice-phase precipitation liquid-equivalent drop-size distribution parameters ($\log(N_w)$, D_o, μ) along the Ku/Ka ray at 250 m sampling resolution (2 byte integer. nPSD x nbinC x nrayS2 x nscan); from the 2BCMB Combined Algorithm (in S2).

icePSDparamSigmaOut
ice-phase precipitation liquid-equivalent drop-size distribution parameter ($\log(N_w)$, D_o, μ) uncertainties along the Ku/Ka ray at 250 m vertical resolution (2 byte integer, nPSD x nbinC x nrayS2 x nscan); from the 2BCMB Combined Algorithm (in S2).

iceDensityOut
density of ice-phase precipitation expressed as a power law (α, β, of $\rho_{ice} = \alpha D^{\beta}$, where D is particle melted diameter) along the Ku/Ka ray at 250 m sampling resolution (2 byte integer, nAB x nbinC x nrayS2 x nscan); from the 2BCMB Combined Algorithm (in S2).

iceMeltFractionOut
fraction of melting ice particle liquid-equivalent water content in the form of liquid water along the Ku/Ka ray at 250 m sampling resolution (2 byte integer, nbinC x nrayS2 x nscan); from the 2BCMB Combined Algorithm (in S2).

surfRainRateOut
surface liquid precipitation rate at Ku/Ka footprint location (4 byte float, nrayS2 x nscan); from the 2BCMB Combined Algorithm (in S2).

surfRainRateSigmaOut

surface liquid precipitation rate uncertainty at Ku/Ka footprint location (4 byte float, nrayS2 x nscan); from the 2BCMB Combined Algorithm (in S2).

surfPrecipIceRateOut
surface ice-phase precipitation rate at Ku/Ka footprint location (4 byte float, nrayS2 x nscan); from the 2BCMB Combined Algorithm (in S2).

surfPrecipIceRateSigmaOut
surface ice-phase precipitation rate uncertainty at Ku/Ka footprint location (4 byte float, nrayS2 x nscan); from the 2BCMB Combined Algorithm (in S2).

tenMeterWindSpeedOut
10-meter wind speed at Ku/Ka footprint location (4 byte float, nrayS2 x nscan); from the 2BCMB Combined Algorithm (in S2).

surfaceEmissivityOut
microwave surface emissivities at the GMI channel frequencies/polarizations and viewing angle, including separate emissivities for the double side-band channels at 183.3 ± 7 and 183.3 ± 3 GHz, at Ku/Ka footprint location (4 byte float, nchan x nrayS2 x nscan); from the 2BCMB Combined Algorithm (in S2).

simulatedBrightTempOut
upwelling microwave surface brightness temperatures at the GMI channel frequencies/polarizations and viewing angle, but at Ku/Ka footprint resolution, including separate brightness temperatures for the double side-band channels at 183.3 ± 7 and 183.3 ± 3 GHz (4 byte float, nchan x nrayS2 x nscan); from the 2BCMB Combined Algorithm (in S2).

piaOut
total path-integrated attenuations at the Ku and Ka band (4 byte float, nKuKa x nrayS2 x nscan); from the 2BCMB Combined Algorithm (in S2).

correctedReflectFactorOut
attenuation-corrected radar reflectivity factor at Ku and Ka band at 250 m sampling resolution (2 byte integer, nKuKa x nbinC x nrayS2 x nscan); from the 2BCMB Combined Algorithm (in S2).

Output Parameters (Near Real-Time Processing)

from the 2BCMB Combined Radar-Radiometer Algorithm (S1)

Year
year of the Ku band scan (2 byte integer, nscan); from the 2BCMB Combined Algorithm (in S1).

Month
month of the Ku band scan (1 byte integer, nscan); from the 2BCMB Combined Algorithm (in S1).

DayOfMonth
day of month of the Ku band scan (1 byte integer, nscan); from the 2BCMB Combined Algorithm (in S1).

Hour
hour of the Ku band scan (1 byte integer, nscan); from the 2BCMB Combined Algorithm (in S1).

Minute
minute of the Ku band scan (1 byte integer, nscan); from the 2BCMB Combined Algorithm (in S1).

Second
second of the Ku band scan (1 byte integer, nscan); from the 2BCMB Combined Algorithm (in S1).

MilliSecond
millisecond of the Ku band scan (2 byte integer, nscan); from the 2BCMB Combined Algorithm (in S1).

DayOfYear
day of year of the Ku band scan (2 byte integer, nscan); from the 2BCMB Combined Algorithm (in S1).

SecondOfDay
second of day of the Ku band scan (8 byte float, nscan); from the 2BCMB Combined Algorithm (in S1).

Latitude
latitude of Ku band footprint (4 byte float, nrayS1 x nscan); from the 2BCMB Combined Algorithm (in S1).

Longitude
longitude of Ku band footprint (4 byte float, nrayS1 x nscan); from the 2BCMB Combined Algorithm (in S1).

surfaceElevation
altitude above the Earth ellipsoid of the surface gate in Ku band ray (4 byte float, nrayS1 x nscan); from the 2BCMB Combined Algorithm (in S1).

surfaceType
water/land/coast and surface type at Ku band footprint location (4 byte integer, nrayS1 x nscan); from the 2BCMB Combined Algorithm (in S1).

precipitationType
classification of precipitation type in Ku band ray (4 byte integer, nrayS1 x nscan); from the 2BCMB Combined Algorithm (in S1).

precipTypeQualityFlag
quality of classification of precipitation type in Ku band ray (4 byte integer, nrayS1 x nscan); from the 2BCMB Combined Algorithm (in S1).

surfRainRateOut
surface liquid precipitation rate at Ku footprint location (4 byte float, nrayS1 x nscan); from the 2BCMB Combined Algorithm (in S1).

surfRainRateSigmaOut
surface liquid precipitation rate uncertainty at Ku footprint location (4 byte float, nrayS1 x nscan); from the 2BCMB Combined Algorithm (in S1).

surfPrecipIceRateOut
surface ice-phase precipitation rate at Ku footprint location (4 byte float, nrayS1 x nscan); from the 2BCMB Combined Algorithm (in S1).

surfPrecipIceRateSigmaOut
surface ice-phase precipitation rate uncertainty at Ku footprint location (4 byte float, nrayS1 x nscan); from the 2BCMB Combined Algorithm (in S1).

from the 2BCMB Combined Radar-Radiometer Algorithm (S2)

Year
year of the Ku/Ka scan (2 byte integer, nscan); from the 2BCMB Combined Algorithm (in S2).

Month
month of the Ku/Ka scan (1 byte integer, nscan); from the 2BCMB Combined Algorithm (in S2).

DayOfMonth
day of month of the Ku/Ka scan (1 byte integer, nscan); from the 2BCMB Combined Algorithm (in S2).

Hour
hour of the Ku/Ka scan (1 byte integer, nscan); from the 2BCMB Combined Algorithm (in S2).

Minute
minute of the Ku/Ka scan (1 byte integer, nscan); from the 2BCMB Combined Algorithm (in S2).

Second
second of the Ku/Ka scan (1 byte integer, nscan); from the 2BCMB Combined Algorithm (in S2).

MilliSecond
millisecond of the Ku/Ka scan (2 byte integer, nscan); from the 2BCMB Combined Algorithm (in S2).

DayOfYear
day of year of the Ku/Ka scan (2 byte integer, nscan); from the 2BCMB Combined Algorithm (in S2).

SecondOfDay
second of day of the Ku/Ka scan (8 byte float, nscan); from the 2BCMB Combined Algorithm (in S2).

Latitude
latitude of Ku/Ka footprint (4 byte float, nrayS2 x nscan); from the 2BCMB Combined Algorithm (in S2).

Longitude
longitude of Ku/Ka footprint (4 byte float, nrayS2 x nscan); from the 2BCMB Combined Algorithm (in S2).

surfaceElevation
altitude above the Earth ellipsoid of the surface gate in Ku/Ka ray (4 byte float, nKuKa x nrayS2 x nscan); from the 2BCMB Combined Algorithm (in S2).

surfaceType

water/land/coast and surface type at Ku/Ka footprint location (4 byte integer, nrayS2 x nscan); from the 2BCMB Combined Algorithm (in S2).

precipitationType
classification of precipitation type in Ku/Ka ray (4 byte integer, nrayS2 x nscan); from the 2BCMB Combined Algorithm (in S2).

precipTypeQualityFlag
quality of classification of precipitation type in Ku/Ka ray (4 byte integer, nrayS2 x nscan); from the 2BCMB Combined Algorithm (in S2).

surfRainRateOut
surface liquid precipitation rate at Ku/Ka footprint location (4 byte float, nrayS2 x nscan); from the 2BCMB Combined Algorithm (in S2).

surfRainRateSigmaOut
surface liquid precipitation rate uncertainty at Ku/Ka footprint location (4 byte float, nrayS2 x nscan); from the 2BCMB Combined Algorithm (in S2).

surfPrecipIceRateOut
surface ice-phase precipitation rate at Ku/Ka footprint location (4 byte float, nrayS2 x nscan); from the 2BCMB Combined Algorithm (in S2).

surfPrecipIceRateSigmaOut
surface ice-phase precipitation rate uncertainty at Ku/Ka footprint location (4 byte float, nrayS2 x nscan); from the 2BCMB Combined Algorithm (in S2).

Appendix B. Output Product Volumes

The volume of the Combined Algorithm standard output product, based upon the output parameters listed above, is approximately 2.3 GB per orbit assuming 7900 DPR scans per orbit. Since precipitation only occurs over 5-10% of the earth's surface at any particular time, many of the precipitation parameters in the output product will be either zero or a flagged as missing; therefore, the output product files are expected to compress by a factor of 10, at least.

To facilitate internet transfer of data, the Combined Algorithm near real-time product is much smaller; about 25 MB per orbit. This reduced product retains only the surface precipitation rates and their uncertainties.

Appendix C. Processing Requirements

The current configuration of the Combined Algorithm will require input from five modules of the GPM Radar Algorithm: the Preparation Module, Vertical Profile Module, Classification Module, DSD Module, and Surface Reference Technique Module. Output of these modules is expected from the Level 2 Radar Algorithm software; however, the computational requirements of this routine could add significant latency to Combined Algorithm processing.

A primary input to the Vertical Profile Module will be JMA global analyses (GANAL) for standard processing and JMA global analyses/forecasts for near-real-time processing. Therefore, this input should be accommodated in PPS operations.

The current version of the algorithm requires approximately 6 minutes on a single processor to process 3000 PR footprints. A typical orbit of DPR data will have 20,000 – 30,000 rain-affected footprints. This indicates roughly 60 minutes processing time per orbit using a single processor. Although some economies in the coding can reduce this processing time, they may result in degraded performance of the algorithm. The preferred alternative is to use multi-processing capability at PPS with the equivalent of ~10 CPU to reduce the overall processing time to 6 minutes/orbit. Granules of DPR and GMI data will be subdivided into (300 DPR scan line) segments that will be processed in parallel. Parallel processing will be achieved using POSIX thread libraries.